SEPARATION OF REGIONAL AND RESIDUAL COMPONENTS OF BATHYMETRY USING DIRECTONAL MEDIAN FILTERING

A THESIS SUBMITTED TO THE GRADUATE DIVISION OF THE
UNIVERSITY OF HAWAI'I IN PARTIAL FULFILLMENT
OF THE REQUIREMENTS FOR THE DEGREE OF

MASTER OF SCIENCE

IN

GEOLOGY AND GEOPHYSICS

AUGUST 2005

By
Seung-Sep Kim

Thesis Committee:

Paul Wessel, Chairperson
Fred K. Duennebier
John J. Mahoney

We certify that we have read this thesis and that, in our opinion, it is satisfactory in scope and quality as a thesis for the degree of Master of Science in Geology and Geophysics.

THESIS COMMITTEE

_____

Chairperson

_____

_____

Abstract

I propose a new filtering technique to separate bathymetric data into regional and residual components. Directional median (DiM) filtering divides a given filter circle into N "bow-tie" sectors, allocates the data points inside the filter circle to each bow-tie sector based on their relative position with respect to the center of the filter circle, estimates a median value for each sector, and returns the lowest of these median values. This procedure is introduced to circumvent a shortcoming of conventional median filters, which return biased median estimates for data exhibiting short-length-scale features (e.g., seamounts) superimposed on sloping backgrounds (e.g., swells or slopes caused by thermal subsidence of lithosphere). By preserving the robust properties of spatial median filters and overcoming the limitation mentioned above, DiM filtering is able to efficiently isolate short-length-scale features from sloping regional components. Because DiM filtering results depend on the choice of filter width, I find effective filter widths, a range of filter widths enabling DiM filters to remove the given short-length-scale features completely, based on both the ratio of the volume to the area of estimated residual components and the width of the largest feature in the data domain. Furthermore, uncertainties in the predicted regional component are quantified by estimating median absolute deviation (MAD) values at each data point, which evaluate whether the DiM filters produce similar regional components within the chosen effective filter widths. The distribution of MAD values, therefore, can be used to identify the causes of large fluctuations in regional components and suggest ways to reduce these variations. The DiM filtering with associated MAD analysis is applied to both synthetic and actual bathymetric data of the seafloor around the Easter-Salas y Gomez Seamount Chain and the Cape Verde Islands. These tests confirm that the DiM filtering allows researchers to prepare suitable input data (e.g., residual components used as applied loads in flexural studies) and quantify the uncertainties.

Contents

List of Tables

List of Figures

Chapter 1

Introduction

Earth scientists often observe the net effect of various geological phenomena. In order to understand the nature of a particular phenomenon, one must decide how to separate a portion of the data thought to represent the phenomenon from the rest of the data. A proper method will be chosen based on the properties of the data and the feature of interest. A geochemist, for instance, needs to know a reasonable baseline level (i.e., a normal level, concentration, or ratio) for results analyzed in a laboratory so that she or he can isolate the effect of the feature from the rest of the observations. In geophysical studies, bathymetric highs (e.g., seamounts and swells) on oceanic plates are often of prime interest. Seamounts (including oceanic islands) represent evidence indicating how the lithosphere responds to long-term volcanic loads, a phenomenon widely modeled using flexure theory [e.g., *McNutt and Menard*, 1978; *Lambeck and Nakiboglu*, 1980; *Kruse et al.*, 1997; *Ali et al.*, 2003]. Whereas the flexural model parameters can be constrained with other geophysical observations (e.g., free-air gravity anomalies), the surface loads causing the deformation can be inferred only from bathymetric data and hence one needs to isolate the residual components (i.e., seamounts) from the bathymetric background [e.g., *Wessel*, 1993; *Ali et al.*, 2003]. Swells, however, are the surface manifestations induced by buoyant mantle upwelling (i.e., hot spots or mantle plumes) [e.g., *Crough*, 1983; *McNutt*, 1998]. To estimate volume fluxes of hot spot material, the shape of the broad bathymetric feature (i.e., regional component) is a crucial model constraint [e.g., *White*, 1993; *Vidal and Bonneville*, 2004; *Van Ark and Lin*, 2004]. Therefore, the focus of this study is on (i) bathymetric data that may have features of different length scales (e.g., seamounts and swells) overlapping in the spatial domain, and (ii) an effective and efficient method to separate the regional and

residual components from the bathymetric data.

To facilitate this process, known as regional-residual separation [e.g., *Telford et al.*, 1986], various methods have been proposed and employed. In the most straightforward approach, the separation of profile data can be achieved graphically by a researcher's hand drawing [e.g., *Nettleton*, 1976]. This manual interpretation technique allows one to use additional information (e.g., seismic profiles) for the analysis and to inspect the results visually and simultaneously. These merits can make for a rapid separation process if the data are of a manageable size (e.g., a few single-beam or potential field profiles). This method, however, does not quantify the criteria for the analysis and thus may produce biased results because of the personal opinions of the practitioner. As the method is subjective, it generally does not result in consistent answers. Finally, it is less suitable for map data. Another approach is to employ low-pass filters with the assistance of the fast Fourier transform [e.g., *Lambeck*, 1981]. The low-pass filtering method bases the separation on the assumption that the residual and regional components of data will have different wavelengths; hence, one can suppress wavelengths assumed to represent the regional components. Despite its well-quantified procedures, this technique often produces incomplete separations because of overlap between the residual and regional components in the Fourier domain. In particular, the irregular and rough nature of bathymetric features leads to very broad spectra, resulting in difficulties when attempting to distinguish between the components in the Fourier domain and, consequently, yielding unsatisfactory separations [*Wessel*, 1998; *Adam et al.*, 2005]. An alternative approach is derived from the spatial filtering, such as mode [*Levitt and Sandwell*, 1996; *McNutt et al.*, 1996] and median [*Smith*, 1990; *Wessel*, 1998] filters. Their most valuable property in data analysis is the insensitivity to outliers, i.e., data points far from most others in a set of data. This property (herein called robustness) of both filters often enables one to find reproducible and satisfactory regional bathymetric components. However, the

slopes inherent in bathymetric data introduce complications in both the mode and median filtering analyses [*Smith*, 1990; *Wessel*, 1998]. In this study, the problems associated with the conventional median filters will be investigated.

The principles of the above methods are utilized in three newly developed techniques: the micro macro interpretation construct (MiMIC) [*Hillier and Watts*, 2004], the multiscale vision model (MVM) [*Starck et al.*, 2000], and the minimization and filtering (MiFil) method [*Adam et al.*, 2005]. The MiMIC method removes all small-scale (e.g., seamounts and aseismic ridges) and medium-scale (e.g., oceanic plateaus and hot spot swells) bathymetric features, in order to isolate large-scale features (e.g., superswells). The main operations of MiMIC are the search construct and morphological assessment. The search construct is a process to find bathymetric highs (e.g., seamounts) within a given search range along a depth profile. When a high is found, the morphological assessment rejects it if the skewness and average height of the detected high do not fall into the empirically determined range of each shape parameter, or divides it into multiple geological features according to the "up-warp" test. For more details, see *Hillier and Watts* [2004]. These complicated tests are developed in order to simulate manual interpretation, however they also introduce difficulties for researchers to apply MiMIC to different data sets. Furthermore, MiMIC is unable to distinguish seamounts from narrow ridges in a given data set, because it operates on 2-D depth profiles only.

The MVM technique decomposes a photograph of numerous stars and galaxies taken by a telescope into individual objects using the wavelet transform, whose characteristics prevent the objects from overlapping in wavelet space. Although bathymetric and astronomical data share some similarities, the behavior of noise sources in MVM associated with photometry is very different from those associated with bathymetric data. MVM detects an object if the absolute value of its wavelet coefficient is above a given detection limit. The detection limit depends on the noise model (e.g.,

Gaussian noise model). Therefore, implementing MVM for use with geophysical data needs further investigation (i.e., noise modeling).

MiFil is different from the above new methods, both of which approach data as a hierarchically organized structure, in that MiFil combines two spatial filters in order to define the shape of swells. In this method, a depth anomaly grid is obtained by subtracting the predicted depth based on the GDH1 thermal subsidence model [*Stein and Stein*, 1992] from the bathymetric data. Next, a "minimizing filter" removes short-length-scale features from the depth anomaly grid. At each point of the grid, the minimizing filter returns the minimum value (i.e., maximum depth in the bathymetry) inside the filter circle. Finally, a spatial median filter smooths the minimized data and eliminates the remainder of the short-length-scale features. The reason to apply the minimizing filter is to reduce biased median filtering results around the short-length-scale features superimposed on sloping backgrounds [e.g., *Smith*, 1990; *Wessel*, 1998]. In order to achieve this goal, the minimized data must exhibit much smaller features than those in the input grid (i.e., depth anomaly grid). However, the filter widths for the minimizing filter are mainly limited by the presence of fracture zones. Because the troughs of the fracture zones are always deeper than the surrounding seafloor, the minimizing filter with larger filter widths actually widen the troughs and hence short filter widths (e.g., 15 km) are chosen for the filter. Large features on sloping backgrounds, however, cannot be significantly minimized with their short filter widths. Consequently, the second stage of the MiFil method (i.e., the median filter) still has difficulty handling sloping backgrounds, thus forcing a practitioner to choose median filter widths wider than the reasonable choice [e.g., *Minshull and Charvis*, 2001; *Ali et al.*, 2003].

I seek an efficient and effective way to separate bathymetric data into regional and residual components using as little additional constraints as possible. In many instances, data sets are often limited by both quality and coverage. Using several

criteria in the separation, moreover, makes arriving at reasonable results more complicated and requires a user to have broad experience with data from many provinces. Thus, although the new methods discussed above remedy some of the shortcomings of the traditional approaches, they are not compatible with the requirements of this study. Instead, I shall make use of spatial median filters and take advantage of their ease of use and simplicity of operation. In this study, a new median filtering scheme is developed and used to define a regional component compatible with manual interpretation of data consisting of short-length-scale features and sloping backgrounds. The observed bathymetric data are the sum of many different geologic processes, however there is not enough information to separate the data into each component. Thus, the new filtering method defines a regional component by removing short-length-scale features from the given bathymetric data and then considers the removed data by filtering as a residual component. Unlike all previous studies, my method estimates uncertainties in the analyzed results. Finally, this scheme is applied to real bathymetric data in the vicinity of the Easter-Salas y Gomez Seamount Chain and the Cape Verde Islands, and comparisons are made with published results.

Chapter 2

Directional Median (DiM) Filter

2.1 Basics of Median Filters

The exceptional characteristic of median filters that makes them so suitable for the regional-residual separation task is their insensitivity to outliers; this is attained by searching for the middle value of all data points inside the filter diameter [*Davis*, 1986]. This property has been demonstrated in various fields of data analysis, particularly in studies that involve smoothing noisy observations and improving images. *Wessel* [1998] discussed the nature of median filters as applied to bathymetric features. For a given filter width, a median filter removes short-length-scale features like a conventional low-pass filter. However, the median filter does not specify a spectral representation (i.e., its effects at different wavelengths) for the features of interest; thus it can only be formulated in the spatial domain. The filtered data reflect the general background trend (i.e., regional component) of the given data set. Thus, high-pass median filtering to isolate the short-length-scale features (i.e., residual component) is simply achieved by subtracting the median-filtered data from the original observations. The important effect of median filters on 2-D and 3-D data is that any feature can be removed completely if a filter is wide enough to always include more data points from the background than the feature itself [*Wessel*, 1998]. For 3-D data, in particular, this can be established from the rule of thumb that "the filter area must be at least twice the feature area," which can be written as

$$W \geq \sqrt{2}D. \tag{2.1}$$

Here, W is the filter width of a median filter and D the diameter of a feature. Using this rule ensures that more than half of the data given to the median filter come from the background, and enables a median filter to return median values reflecting the background trend at each data point, even at points directly beneath the short-length-scale feature. Thus, the feature will be removed completely after filtering. For instance, Figure 2.1 illustrates a snapshot of the actual median filtering process on a small cylinder of radius $r = 2$ and height $h = 3$, which is placed on a flat background (upper panel). From (2.1), a filter width of $W = 6$ is chosen. The histogram in the lower panel represents the number of data points from each component (i.e., background and feature) inside the filter circle (solid line in the upper panel), when the filter is centered at $(0, 0)$. The dashed line indicates 50% of the total data points and hence the median value beneath the feature is determined by one of the background data. Therefore, one can expect a median filter to remove efficiently the short-length-scale feature from the input data by choosing a filter width based on (2.1). I will call this filter width as an "effective" filter width because it is necessary for median filters to produce the results that were intended (i.e., complete removal of short-length-scale features). The details regarding the choice of filter width are discussed in the following section.

However, it turns out that this property fails to define a proper regional components when the data are composed of short-length-scale features superimposed on a gently inclining background. The profiles in Figure 2.2a are typical of the separation achieved by median filters. The synthetic data (solid line and circles) comprise a short-length-scale feature (diameter $D = 6$) superimposed on a constant (upper panel) or sloping (lower panel) background. The median filter, with its effective filter width, $W = 12$, is able to estimate a regional component identical to the original background (dashed line and open circles) only for the flat case in the upper panel. The same filter in the lower panel fails to find the middle value of the monotonically

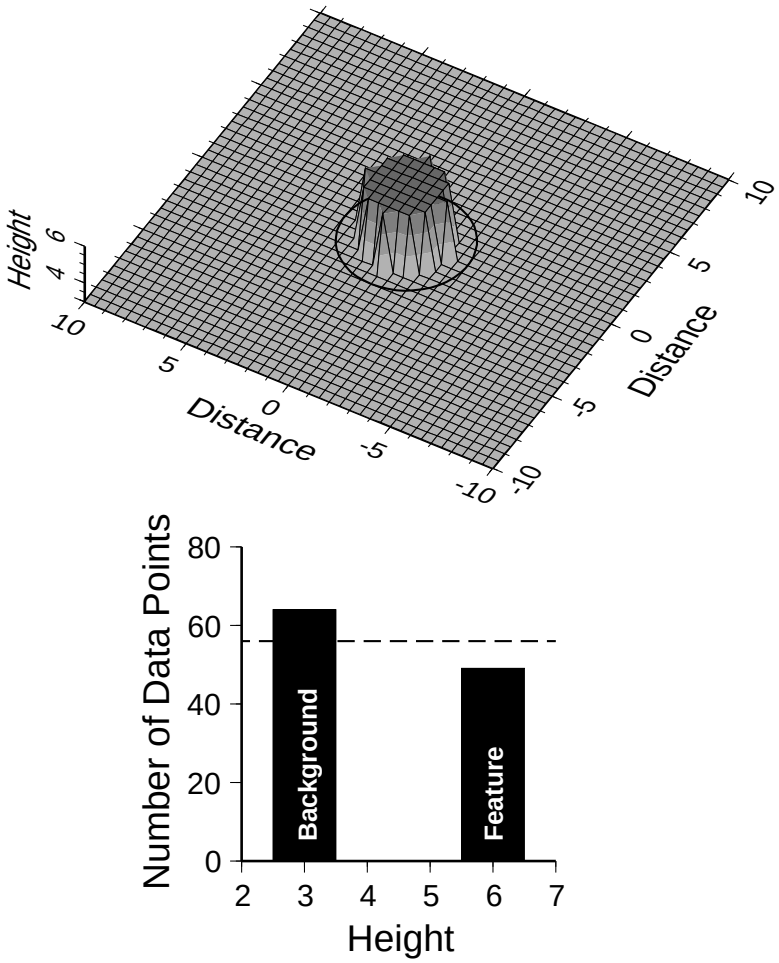

Figure 2.1: Snapshot of the median filtering process. A cylinder of radius $r = 2$ and height $h = 3$ is placed on a flat background (upper panel). An effective filter width of $W = 6$ is chosen to always contain more data points from the background data than the feature itself. For instance, the histogram in the lower panel represents how many points from each source are given to the filter, when the filter circle is centered at $(0, 0)$. As expected, more than half of data points (indicated by the dashed line) are from the background data. Thus, the median value beneath the cylinder is obtained from the background data. When the filter is centered elsewhere, the background will dominate even more. Units for distance and height are arbitrary.

increasing trend around the feature. In this case, the filter operates on both significantly varying data points from both the feature and the background, so that the median values are pulled up toward the feature. Obviously, the median filter can accurately recover this sloping trend only if the short-length-scale feature does not exist or a much wider filter width is employed to include more data points from the background. However, estimating background trends in the presence of short-scale features is the purpose of the separation. To enlarge the filter width, we would need to assume that the slope in the given data is constant. However, this assumption complicates the choice of filter width because it is very difficult to predict both how much median values will be biased by the slope and how fast the biased median values will be reduced by enlarging the filter width. Furthermore, a constant slope is rarely the case in reality. The failure to remove a feature on a sloping background is also found in 3-D data sets. For instance, a cone is placed on top of the inclined plane (Figure 2.2b), whose length scale and slope are the same as those of the lower panel in Figure 2.2a. The spatial median filter with the same effective filter width that succeeded in the case of the flat trend results in a biased regional component having a "pull-up" pattern (Figure 2.2c).

Median filters reproduce the characteristics in Figure 2.2a with real geophysical data sets. Because the wide Hawaiian Swell is seen as a slowly varying background (e.g., upper panel) beneath the Hawaiian Islands, the separation achieved by *Wessel* [1998] was fortuitously successful. However, relatively small swells (e.g., lower panel) introduce the same problems in the separation and typically lead to compromises such as using filter widths wider than the effective widths [e.g., *Minshull and Charvis*, 2001; *Ali et al.*, 2003]. One practical remedy to this problem is to estimate a best-fitting plane that approximates the slope of the data inside the filter window; it can then be removed from the data before the median filter is applied and later added back to the filtered data [*Wessel*, 1998]. However, it is very difficult to describe the complex

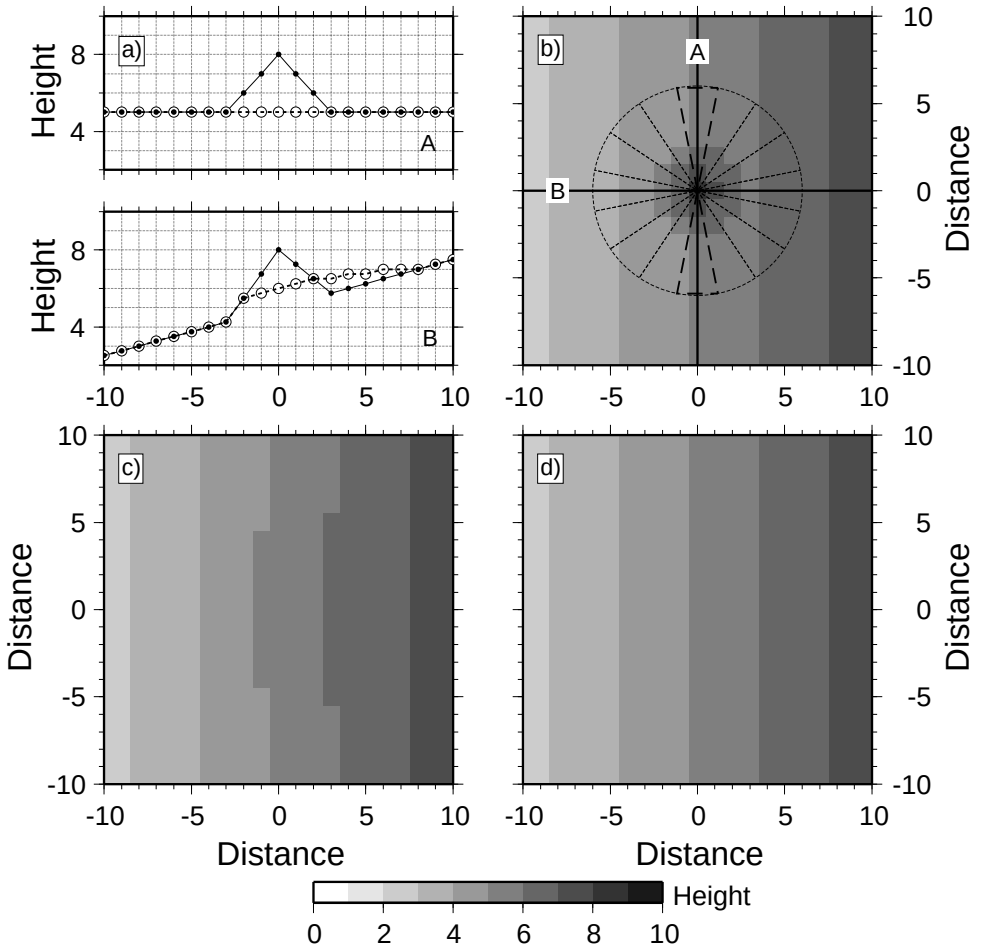

Figure 2.2: Illustration of the DiM (directional median) filtering technique. a) Failure of a median filter to remove a feature on a slope. Based on Fig 4. of *Wessel* [1998], the panels show the unsuitable separation produced by the median filter ($W = 12$) for a feature superimposed on a sloping background (profile B). Solid line and circles are the input and dashed line and open circles reflect the median filter output. b) The 3-D synthetic data consisting of a cone and inclined plane are shown. To avoid a biased median value at $(0\,,0)$ due to the slope, the DiM filter divides its filter circle ($W = 12$) into eight bow-tie sectors (thin dashed lines), estimates median values of data within each sector, and returns the minimum median (i.e., deeper value) as the final output. In this way, the DiM filter will succeed because the median values are always pulled up by the feature (as shown in profile B, panel a; solid line), except for the perpendicular bow-tie sector (thick dashed lines). Thus, the DiM filter can determine median values under the favorable condition illustrated in profile A (panel a). c) The pull-up shown in profile B causes errors in the regional component estimated by the spatial median filter. d) The DiM filter recovers the original incline completely. The vertical scale for b), c), and d) is located at the bottom and the units are arbitrary.

trends in bathymetric data using simple least-squares fitting, given its sensitivity to outliers. In the following section, I propose a modification to the general spatial median filter in order to remove short-length-scale features efficiently.

2.2 Directional Median (DiM) Filter

To prevent spatial median filters from being affected by slopes, I take advantage of their highly predictable and reproducible "pull-up" patterns. Let us consider again the 3-D synthetic data (Figure 2.2b). The height and length scale of the cone and the slope of the inclined background in this data set are the same as those of the feature and background in the lower graph of Figure 2.2a. Thus, the profiles along the solid lines intersecting at $(0, 0)$ in Figure 2.2b are identical to the 2-D data sets marked A and B in Figure 2.2a. At this point, searching for the middle value of all data points inside the filter circle (thin dashed circle) is analogous to doing it just along line B. While the median value along line A is still robust, as shown in the upper panel of Figure 2.2a, the filtering result is incomplete due to the "pull-up". From this result, I deduce that the median values will not be biased severely upward over the feature, as long as the filter is able to isolate the data from the sector most perpendicular to the slope (i.e., the sector along the strike of the slope), where the background trend in the filter window is essentially horizontal.

Locating this particular sector is achieved by dividing the filter circle into N "bow-tie" sectors (e.g., thin, dashed lines in Figure 2.2b). Each data point is allocated to one of the N bow-tie sectors on the basis of its relative position within the filter circle. Then, the median filter yields N median estimates, one for each sector. The predictable property of median filters assures that the affected median values will produce "pull-up" patterns of different magnitudes. Thus, the lowest median value among all bow-tie sectors has to be the outcome that best approximates the proper

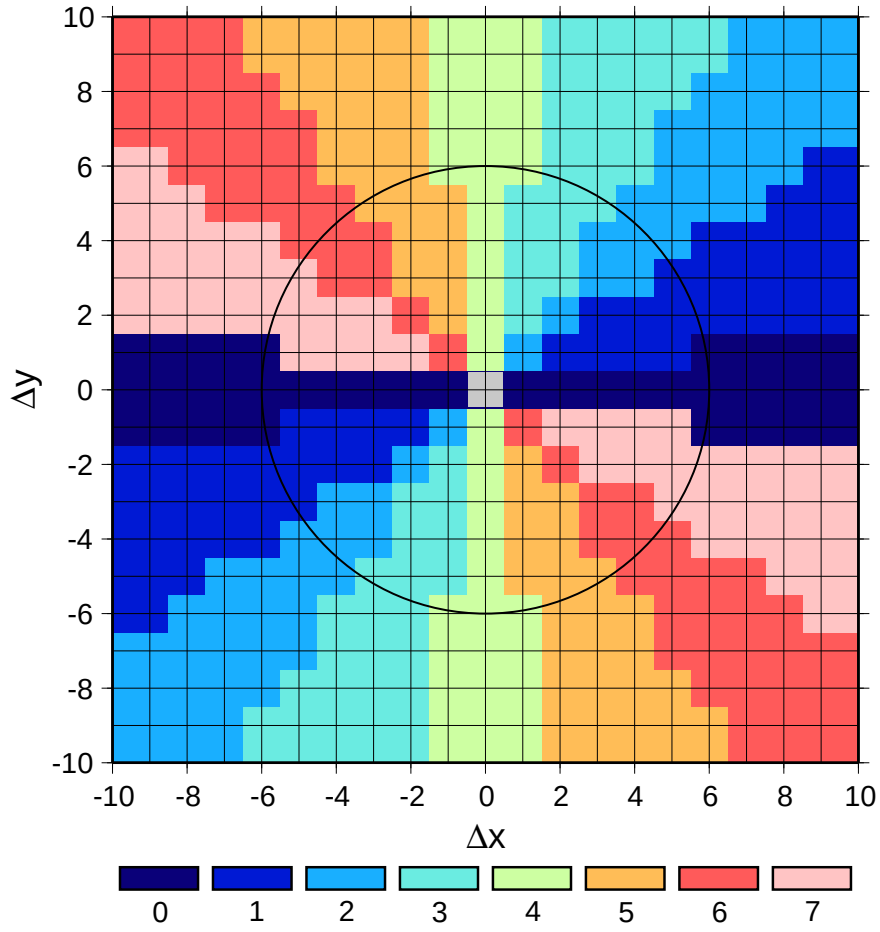

Figure 2.3: Demonstration of bow-tie sectors on a rectangular grid, with $N = 8$. The grid spacing is the same as the gridline spacing of the plot and that of the synthetic data in Figure 2.2. Each data point is allocated to one of the 8 bow-tie sectors (color bar at bottom) by its angle with respect to the center (gray), whose value is assigned to all sectors. The circle (solid line) represents the diameter of the median filter ($W = 12$) used in Figure 2.2. It is inevitable to have an unequal distribution of the data points given to each sector because of the rectangular layout, although the area of each bow-tie sector is equal. DiM filtering searches for the lowest median value from N sectors using only data points within the given filter width (e.g., inside the circle). The choice of N, therefore, involves a trade-off between having enough data points per sector and enough sectors to find the sector most perpendicular to the slope. In this study, $N = 8$ is chosen for DiM filtering on the basis of numerous experiments.

regional elevation, because it is the estimate obtained from the sector along the strike of the sloping plane (e.g., thick dashed lines in Figure 2.2b). As the filtering operation is forced to return median values from data elongated in a certain direction, I call the technique directional median (DiM) filtering. It is programmed in C as a separate tool based on the median filter routine in `grdfilter` of GMT [*Wessel and Smith*, 1995].

The effectiveness of DiM filtering for regional-residual separation depends on both choices of filter width and N. Filter widths enabling DiM filters to remove short-length-scale features completely from the input data can be determined simply by using the rule of thumb [*Wessel*, 1998]. The underlying condition of DiM filtering is that a median filter with an effective filter width will remove the given short-length-scale features if the background is not sloping. For the DiM filter with the effective filter width, the median filter area is still twice the feature area in each sector, because each sector of the filter circle partitioned by DiM filtering has the same area. In other words, the rule of thumb is also valid for DiM filters and hence the median filtering result of each sector depends solely on whether the background in that sector is inclined. Therefore, the lowest median value, i.e., the outcome of DiM filtering, indicates the most successful removal of the features because the median filter results in "pull-ups" around the features superimposed on the sloping background even if the effective filter width is given (e.g., Figure 2.2a). However, the number of data points given to each sector cannot be equal, although each sector has the same area. The main reason is that most modern bathymetric data are prepared on an evenly spaced rectangular grid (Figure 2.3). For smaller N, there are less choices to find the sector along the strike of the slope. For larger N, too few data points are given to each sector so that each median estimate is statistically insignificant. A finer grid spacing may obviate the problem from using larger N, however it decreases computational efficiency. Therefore, one must make compromises between having enough

data points per sector and enough sectors to sense the direction most perpendicular to the slope. In this study, based on considerable experimentation, I use $N = 8$ bow-tie sectors for DiM filtering. For the synthetic data in Figure 2.2b, this new scheme recovers completely the inclining trend underlying the feature as a regional component (Figure 2.2d).

DiM filtering is tested on two synthetic data sets. To simulate real seafloor, the regional background is calculated from the GDH1 thermal subsidence model [*Stein and Stein*, 1992] based on the digital age grid [*Müller et al.*, 1997] of the Nazca plate, the study area where DiM filtering method will be fully applied later. Figure 2.4a shows elliptical seamounts superimposed on the predicted seafloor of the Nazca plate. In general, the median filter captures the regional component, the gentle slope from the cooling plate model, well (Figure 2.4c). The observed rounding of sharp corners is inevitable for median filters [*Wessel*, 1998]. The median-based regional component (dotted line in Figure 2.4b) along profile AB (Figure 2.4a) exhibits the "pull-up" pattern, bending the contour upward around the seamount (Figure 2.4c). Although the amplitude of the pull-up is very small in this example (because of the gentle slope), it becomes significant for larger features on steeper trends (e.g., the Cape Verde midplate swell). Compared to the regional component from traditional median filtering, the regional component obtained by the DiM filter describes almost exactly the original features of the predicted seafloor and maintains the sharp boundaries of the fracture zones better (Figure 2.4d).

In Figure 2.5a, the Nazca Ridge is simulated as a truncated ridge with several seamounts on the predicted seafloor. Clearly, the DiM filter estimates a regional component (Figure 2.5d) more compatible with the original background (i.e., the predicted seafloor) than the regular median filter (Figure 2.5c). However, the DiM filters shows a predictable pattern along line AB in Figure 2.5a that applies to any ridge. DiM filters assume that the slope inside their filter window is in one direction

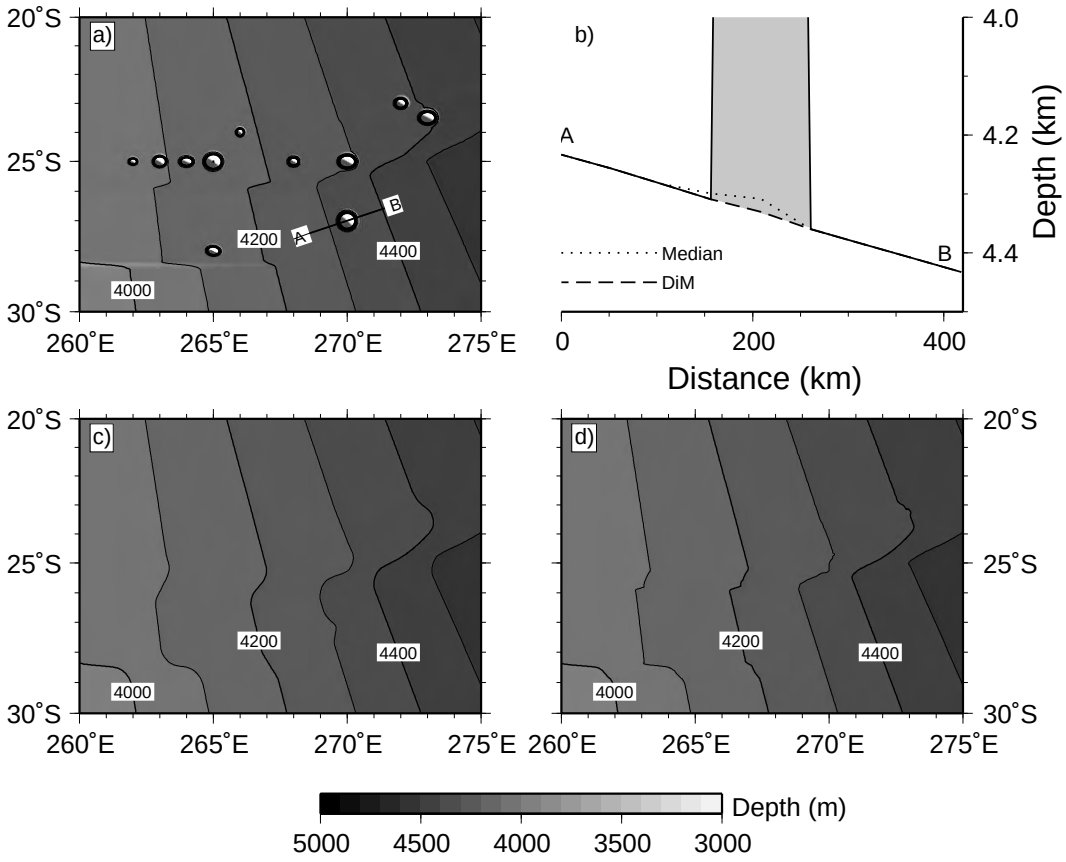

Figure 2.4: Testing DiM filtering on synthetic seamounts superimposed on predicted regional seafloor depth of the Nazca plate. a) The synthetic bathymetry shows Gaussian seamounts on a seafloor whose depth is predicted by the GDH1 model [*Stein and Stein*, 1992], given the digital age grid of *Müller et al.* [1997], simulating thermal subsidence and fracture zones. b) Depth profile AB in a) is compared with the filtered results. The seamount is shaded gray. As shown in Figure 2.2b, the median filter (dotted line) fails to define the expected base of the seamount. c) The median filter results in smooth depth boundaries and artificial bumps in the estimated regional component. d) The DiM filter preserves sharp boundaries better and produces no pull-ups. The effective filter width for both filters is 120 km, 1.5 times the diameter of the largest seamount, as suggested by *Wessel* [1998]. The vertical scale is located at the bottom.

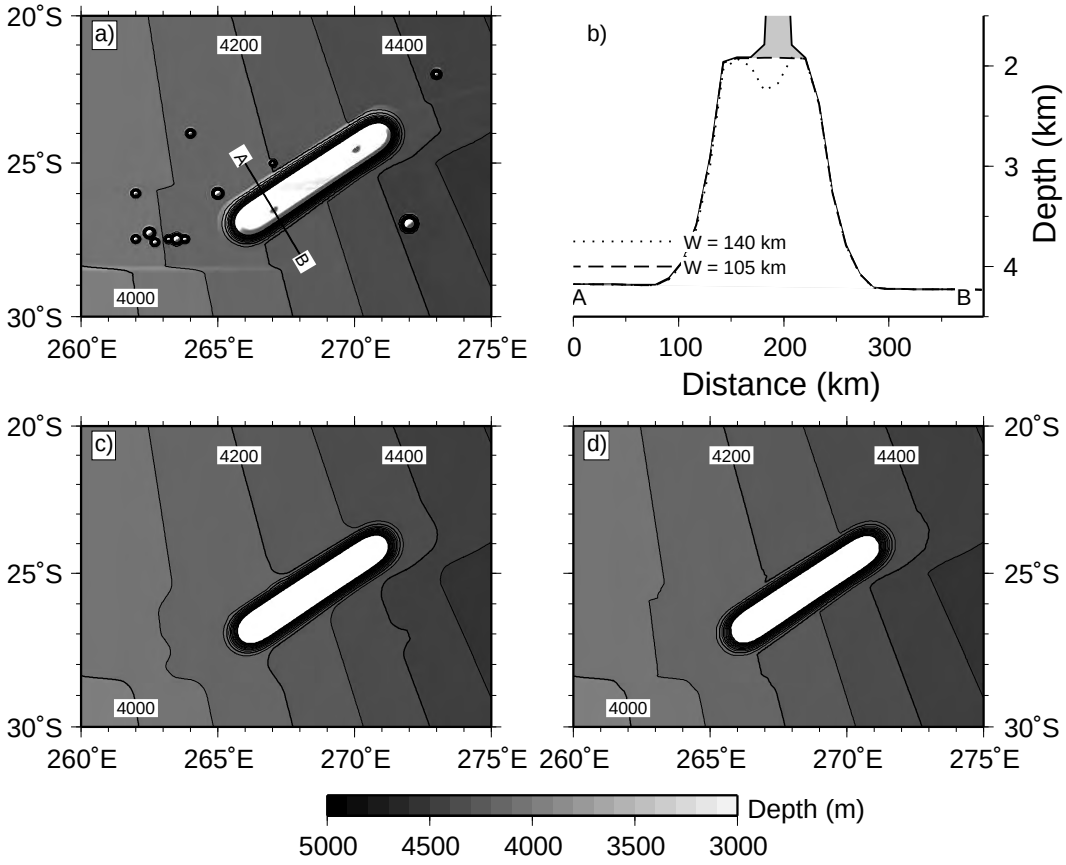

Figure 2.5: Testing DiM filtering on a synthetic ridge and seamounts, superimposed on predicted seafloor depth of the Nazca plate. a) The synthetic bathymetry consists of a truncated ridge and elliptical seamounts on the same seafloor as in Figure 2.4. b) Depth profile AB in a) is compared with the DiM-filtered results of different filter widths. The seamount on the top of the ridge is shaded gray. The dotted line ($W = 140$ km) shows a pull-down of the regional trend at the top of the ridge. The reason is that the DiM filter becomes wide enough to include both slopes inside its filter window. Thus, it returns values from the sector across the ridge (rather than the median values from the sector along the ridge). c) The errors produced by the median filter observed as pull-ups of contours. d) The DiM filter produces sharper boundaries and no pull-ups. The effective filter width for both filters is 105 km, based on the largest seamount in the area. The vertical scale is located at the bottom.

(e.g., because of subsidence of the lithosphere). Mostly, this assumption is valid for most real bathymetric data because the length scales of background features (e.g., swells) are much wider than those of features to be removed (e.g., seamounts). In this synthetic data set, however, the two length scales overlap considerably. At the top of the ridge, the DiM filter will contain data from both slopes of the ridge as the filter width becomes wider than the width of the truncated portion. Thus, the lowest value from the bow-tie sectors is the estimation *not* from the sector along the truncated surface of the ridge (which is desired) but from the sector across the ridge. This caused the "pull-down" along the axis of the ridge (dotted line in Figure 2.5b) when a wider filter width was applied. In reality, volcanic ridges have no fixed width for the truncated top, so that DiM filters for some filter widths may produce such "pull-downs" along the axes.

In addition, the corners of the truncated ridge in Figure 2.5b seem to be preserved well by both DiM and median filters. However, depth profiles of grid data are often obtained by using a interpolating process (e.g., bicubic interpolation). The interpolated data usually exhibit smoother variations than the actual data and hence the rounded corners may not be seen clearly in the profiles if the amount of rounding off is not significant (e.g., Figure 2.5b). Although removing short-length-scale features is of prime interest in regional-residual separation, altering the rest of the data (i.e., regional component) must be limited. In this respect, the median filters round off the corners of both upper (i.e., the tops of the ridge) and lower (e.g., the bases of the ridge) boundaries, whereas the DiM filters only cut off the corners of the upper boundary. Because median filtering use all data points inside the filter circle to find median values, the rounding path is generally smooth [*Wessel*, 1998]. However, the rounding path of DiM filters is straight (e.g., Figures 2.4d and 2.5d).

Clearly, DiM filters can separate short-length-scale features (e.g., seamounts) from both flat (or slowly varying) and sloping backgrounds. This effectiveness of DiM filters

in defining the slopes is an attractive quality that makes it a promising alternative to conventional spatial median filters.

2.3 Error Analysis

Because both DiM and median filters consider only the length scales of the features to be separated, the choice of filter width is closely correlated with the uncertainties of the separation. As mentioned earlier, the effective filter width is necessary to ascertain that the filter circle contains at least twice the feature area. This also can be obtained quantitatively by examining the ratio of the absolute volume of an estimated residual component to its area, referred to as the mean amplitude [*Wessel*, 1998], which is defined by

$$\overline{d} = \frac{V}{A}, \tag{2.2}$$

where the volume V and area A are obtained by

$$\begin{aligned} V &= \int\int_S |d(x,y)|\, dS, \\ A &= \int\int_S dS. \end{aligned} \tag{2.3}$$

Here,

$$d(x,y) = h(x,y) - f(x,y), \tag{2.4}$$

where $d(x,y)$ is an estimated residual component, $h(x,y)$ the observed data, and $f(x,y)$ a regional component obtained by filtering $h(x,y)$. Because of the subtrac-

tion in (2.4), the estimated residual component (e.g., seamounts) will exhibit positive amplitudes. Thus, the volume and area evaluated inside the closed contour $d(x, y) = 0$, defining the domain S, change with respect to filter widths. Note that the estimated residual component may have several unconnected zero-contours if numerous short-length-scale features are found. Figure 2.6 illustrates this concept using spatial median filters to remove a Gaussian feature of radius $r = 30$ km and height $h = 5$ km on a flat background. For example, the volume of the estimated residual component (with $W = 20$ km) is the lightest gray part and the area is equivalent to that of the same gray circle at the bottom. As the filter width is increased, the separation results in rapid increases in both the volume and area of the estimated residual component (see the shaded parts in Figure 2.6). When the filter width is made large enough to remove the feature completely, the volume reaches a maximum while the area only exhibits modest growth. As a result, the mean amplitude ($\overline{d}$) is maximized and the filter width at this moment is an effective width in order for the median filter to remove the feature efficiently. Generally, the volume and area in (2.3) are the sum of contributions from all short-length-scale features in the filtering domain. Therefore, the mean amplitude technique can be applied to real bathymetric data having usually numerous small features. The filter width chosen by the mean amplitude technique is referred to as the optimal robust separator (ORS) in *Wessel* [1998]. However, I still prefer to call it as the "effective" filter width because it is mostly compatible with the width recommended by formula (2.1) and the mean amplitude technique sometimes fails to indicate a unique filter width as discussed below.

Figure 2.7 shows the variations of mean amplitude ($\overline{d}$) for the synthetic data in Figures 2.4 and 2.5 as a function of filter widths. Both the DiM (solid line with triangles) and median (dashed line with circles) filters were used to obtain regional components. The volume and area of the corresponding residual component (2.4) were

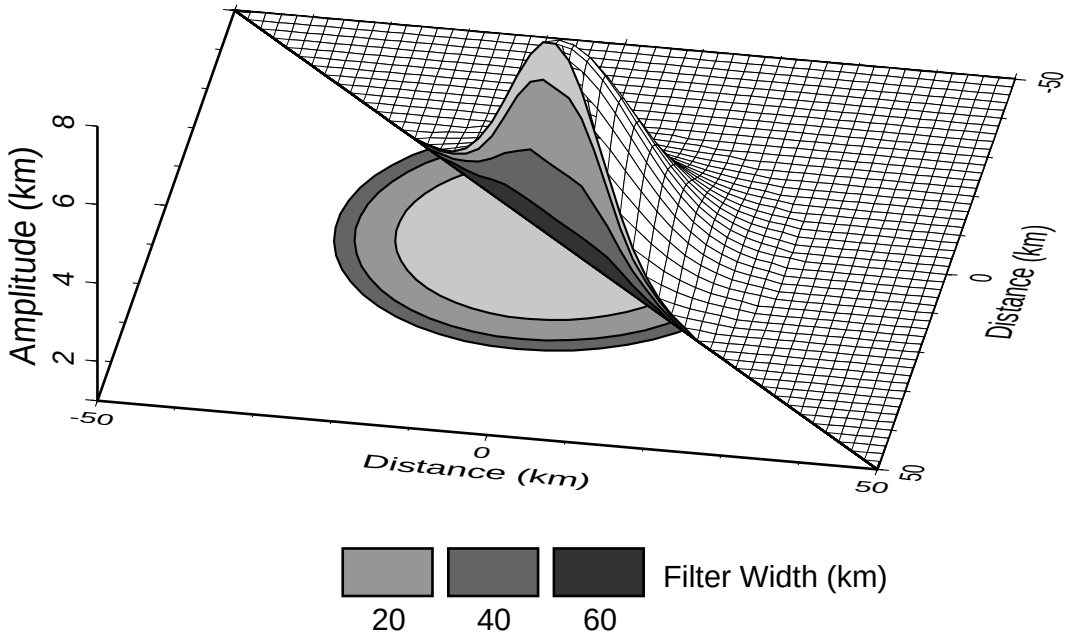

Figure 2.6: Cutaway view of a Gaussian-shaped feature subjected to spatial median filtering. Median filters with different filter widths are applied in order to remove a Gaussian feature of radius $r = 30$ km and height $h = 5$ km. Each filtered result is displayed inside the feature. For example, the median filter with $W = 20$ km removes only the portion filled with the lightest gray. As a result, only this part contributes to the volume and area of the residual. This area is represented as the lightest gray circle at the bottom.

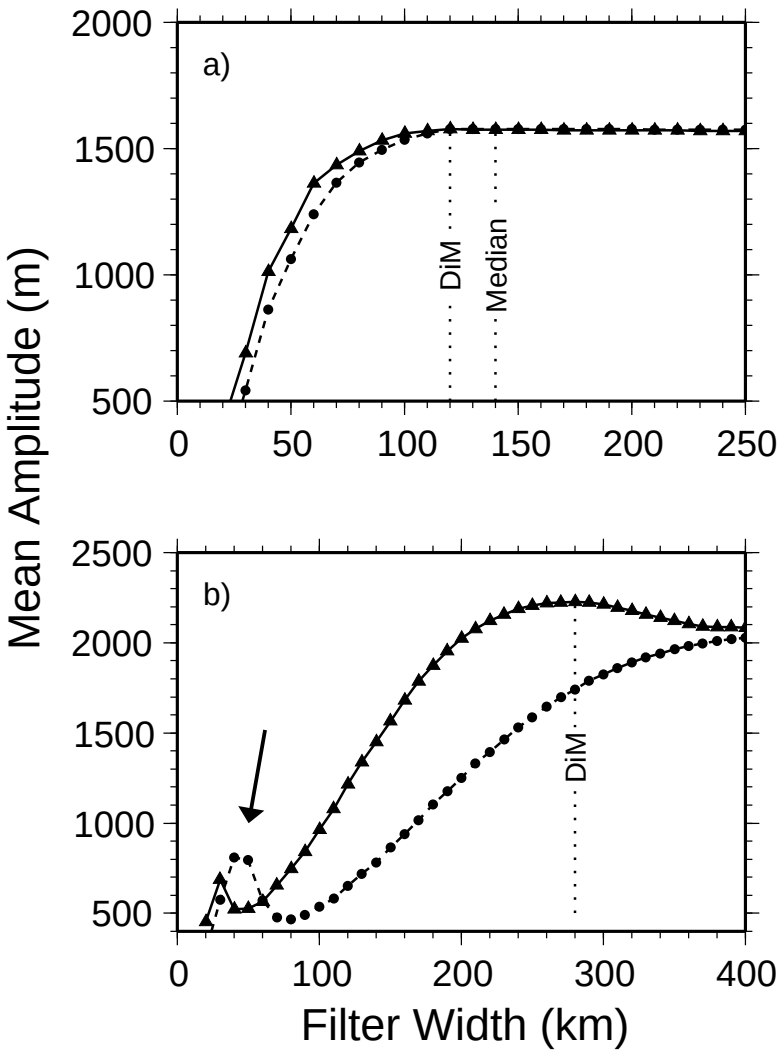

Figure 2.7: Variation of mean amplitude ($\overline{d}$) as a function of filter width for the synthetic data sets in Figures 2.4 and 2.5. Mean amplitudes are calculated from the estimated residual component of each data set obtained by the DiM (solid line with triangles) and median (dashed line with circles) filters. a) Variation of mean amplitude for the synthetic data in Figure 2.4. Effective filter widths are 120 km and 140 km for the DiM and median filters, respectively. Because of the "pull-up" problem, the mean amplitude for median filters reaches the maximum relatively slowly. b) Variation of mean amplitude for the data in Figure 2.5. A unique maximum is found for the DiM filters at $W = 280$ km; however, it is much larger than the previous choice of $W = 105$ km. This inconsistency is mainly a result of the ridge, which also contributes to both the volume and area. The small peaks (arrow) may represent a possible range of filter widths governed only by the small features.

estimated inside the 300 m contour. These synthetic data do not exhibit rough fabrics (e.g., abyssal hills) which are commonly found in real bathymetric data. Because filtered data are generally smoother than such fabrics, residual components derived from real data will exhibit most of this short-length-scale fabric. As a result, the zero contour in the residual will be everywhere. To avoid the excessive meandering of the zero contour and find the basal contours only taking account into the features of interest, the domain S needs to be above the "noise floor" (i.e., the rough fabric of the seafloor). The 300 m level was determined from the standard deviations of bathymetric data for several places in the Pacific and Nazca plates, where no significant bathymetric features (e.g., seamounts) are found. Again, no synthetic data used here have "noise" in them; however, the 300 m level was used in order to verify if this level would influence the mean amplitude technique. For the synthetic data consisting of seamounts and predicted seafloor (Figure 2.7a), the mean amplitude from the DiM filtering is maximized at $W = 120$ km, which is the same as the previous width that produced a suitable regional component (Figure 2.4). The median filter, however, reaches a maximum at $W = 140$ km because the "pull-ups" lead to underestimation of the volume (Figures 2.2a and 2.4b). Thus, the biased separations of median filters would cause one to choose an incorrect effective filter width.

Unfortunately, the mean amplitude technique seems incompatible with the rule of thumb in more complex cases (Figure 2.7b). The synthetic data for Figure 2.5 are composed of two length-scale features; i.e., a ridge and several seamounts. As the filter width is increased, both the DiM and median filters start to remove the ridge and hence a relatively large amount of the volume and area is obtained from the ridge. The small peaks (arrow in Figure 2.7b) may reflect the effects only from the seamounts because the filter widths in that range are too narrow to remove the ridge. Therefore, the DiM filters resulted in an effective filter width ($W = 280$ km), longer than the previous width (i.e., 105 km), wherever the median filters could not

reach a unique maximum in the given range of filter widths. Filter widths larger than 400 km were not considered here because the features of interest (i.e., seamounts) are not in that range (the diameter of the largest seamount is 70 km). As a result of the contributions from the ridge, the mean amplitude is maximized at a filter width that would remove both the ridge and seamounts completely. Because the seamounts are of prime interest in this study, the ridge should not be removed. Although it turns out that the mean amplitude technique is highly dependent on the bathymetry in question, the rule of thumb (2.1) is still valid. In addition to (2.1), selective use of the mean amplitude technique can provide a quantitative measure to confirm the choice of effective filter width. For example, *Wessel* [1998] showed that this approach led to an effective median filter width of 480 km for the test case of the Hawaiian Islands.

In order to minimize computation time, an effective filter width in the present study is the smallest value suggested by either the mean amplitude technique or (2.1). As shown in Figure 2.7a, the mean amplitude technique is unable to determine the upper limit of effective filter widths because the mean amplitude exhibits a flat curve after reaching a maximum. Therefore, a range of effective filter widths, which should give similar filtered results, can be established empirically. For example, the smallest filter width (W_m) may be centered between the upper and lower bounds using a range δW (e.g., ± 25 km). However, whether subjective or objective, the uncertainty in filter widths does not provide any information on the actual changes in the estimated regional and residual components because DiM filters (as well as median filters in general) do not exhibit any mathematical relationship between filter widths and filtered results. That is, "δW km" cannot represent the variation in estimated regional components when a different filter width is used. Instead, I seek the uncertainties of the separation by obtaining a regional component as follows,

1. For each filter width, W_i, determine $f_{W_i}(x, y)$, a DiM-filtered regional component of the bathymetry, $h(x, y)$. W_i is given by

$$W_i = \{W_m - \delta W, \cdots, W_m, \cdots, W_m + \delta W\},$$

in which δW defines the lower and upper bounds. Within the range, the filter widths are required to be incremented using a small interval (e.g., 5 km step), in order to examine enough variations of regional components.

2. Find median values, $\tilde{f}(x, y)$, of all the given estimated regional components at each data point, which can be written

$$\tilde{f}(x, y) = \text{median}\{f_{W_i}(x, y)\}. \tag{2.5}$$

3. Calculate the median absolute deviation (MAD) values, $\tilde{\sigma}(x, y)$, of all the given estimated regional components with respect to $\tilde{f}(x, y)$, at each data point. MAD is defined as [e.g., *Rousseeuw and Leroy*, 1987]

$$\tilde{\sigma}(x, y) = 1.482 \times \text{median}|f_{W_i}(x, y) - \tilde{f}(x, y)|, \tag{2.6}$$

representing the height of fluctuations in the DiM-filtered results at each point with respect to the estimated regional component, $\tilde{f}(x, y)$.

4. Finally, a residual component, $d(x, y)$, is now obtained by subtracting the estimated regional trend, $\tilde{f}(x, y)$, from the observed data, $h(x, y)$. The MAD distribution, $\tilde{\sigma}(x, y)$, can be used to provide upper and lower bounds on the residual component, of the form

$$d(x, y) = h(x, y) - [\tilde{f}(x, y) \pm \tilde{\sigma}(x, y)]. \tag{2.7}$$

In general, the presence of large MAD values associated with a feature means that the DiM filters do not produce stable estimates of the regional component in the range of effective filter widths. One explanation is that no single filter width is ideal for that

feature. In this case, it indicates an underestimation of the volume of the feature. Alternatively and perhaps more likely, it may indicate complicated bathymetry. In any case, one can usually find the reasons for large MAD values by investigating the original bathymetric data. This is another benefit of using DiM filters because the filtered results are not biased by a sloping background, whereas the biased results of the median filters propagate into the mean amplitude analysis. For the cases where the mean amplitude technique fails to provide an effective filter width or the data region in question is relatively large, the MAD analysis will become a crucial tool in order to assess the DiM-filtered results and hence the regional-residual separation.

Chapter 3

Results

In this section, the DiM filtering method is used for regional-residual separation of real bathymetric data and to examine the effectiveness and efficiency of the DiM filters by comparing the results with those estimated by standard spatial median filters.

To verify their enhanced performance compared with conventional median filters, DiM filters are applied to bathymetric data for the vicinity of the Cape Verde Islands (Figure 3.1a). Because the Cape Verde Islands are superimposed on a midplate swell, the bathymetry can be regarded as a combination of short-length-scale features (i.e., the Islands) and a sloping background (i.e., the swell), very similar to the synthetic data in Figure 2.2. The regional-residual separation in this area should display the characteristics of both the DiM and median filters demonstrated on the synthetic data. *Ali et al.* [2003] applied spatial median filters in order to determine the magnitude of the load (i.e., the Cape Verde Islands), which played an important role in the flexural deformation of the Early Cretaceous oceanic lithosphere around the the Cape Verde Islands. Comparison of the result obtained in this study with the published work will confirm if the spatial median filter exhibits the predicted shortcomings (i.e., "pull-up"), and, more fundamentally, if the regional-residual separation by both filters is reproducible.

The predicted bathymetric data (with 2 arc minute, about 2 nautical mile, grid spacing) from satellite altimetry-derived gravity data [*Smith and Sandwell*, 1997] were employed for my regional-residual separation (Figure 3.1a), whereas *Ali et al.* [2003] used the observed bathymetry compiled from shipboard data. In order to directly compare both results, my profile AB (white dashed line) is the same as profile AB in Figure 9 of *Ali et al.* [2003]. The depths in the scale ranges from 6000 m to 2000 m in

order to emphasize the general shape of the Cape Verde swell. However, it is common in filtering map data that the filtered values around the boundary of the map do not represent actual bathymetric trends. The reason is that the filter circle is not filled with data around the edges of the filtering domain. To avoid this "edge effect", the data domain was extended by 5° in all directions beyond the area of interest, and the mean amplitude technique and regional-residual separation were computed only inside the original domain.

The mean amplitude technique was used for a wide range of filter widths, with both the DiM and median filters, in order to determine effective filter widths of the given area (Figure 3.1b). The mean amplitude criterion returned unique maxima at $W = 200$ km (for the DiM filters) and $W = 300$ km (for the median filters); the basic rule (2.1) with the largest diameter of the Islands (about 120 km) recommended an efficient filter width of $W = 180$ km. This inconsistency is very similar to those in Figure 2.7a, representing the "pull-ups" in the median-filtered data. Thus, the mean amplitude analysis returned an effective filter width wider than the recommended width from (2.1). In fact, *Ali et al.* [2003] analysis showed the "pull-up" problem with conventional median filters and hence employed a much wider filter width of $W = 500$ km to capture the Cape Verde swell (see Figure 9 of *Ali et al.* [2003]).

Using the effective filter widths from this study (Figure 3.1b) and from *Ali et al.* [2003], I reproduced their observed "pull-up" and demonstrated the enhanced ability of the DiM filters (Figure 3.2). The presence of noise in the bathymetric data resulting from irregular seafloor fabric induces rough surfaces in the DiM-filtered data. Thus, a secondary regular median filter (with $W = 50$ km) was applied in order to smooth them (Figure 3.2c). Hereafter, the DiM-filtered results are all subjected to this smoothing process (with $W = 50$ km). As mentioned earlier, the removal of short-length-scale features (i.e., seamounts) must not affect the rest of the observations. Therefore, one can assess the separation result indirectly by comparing the

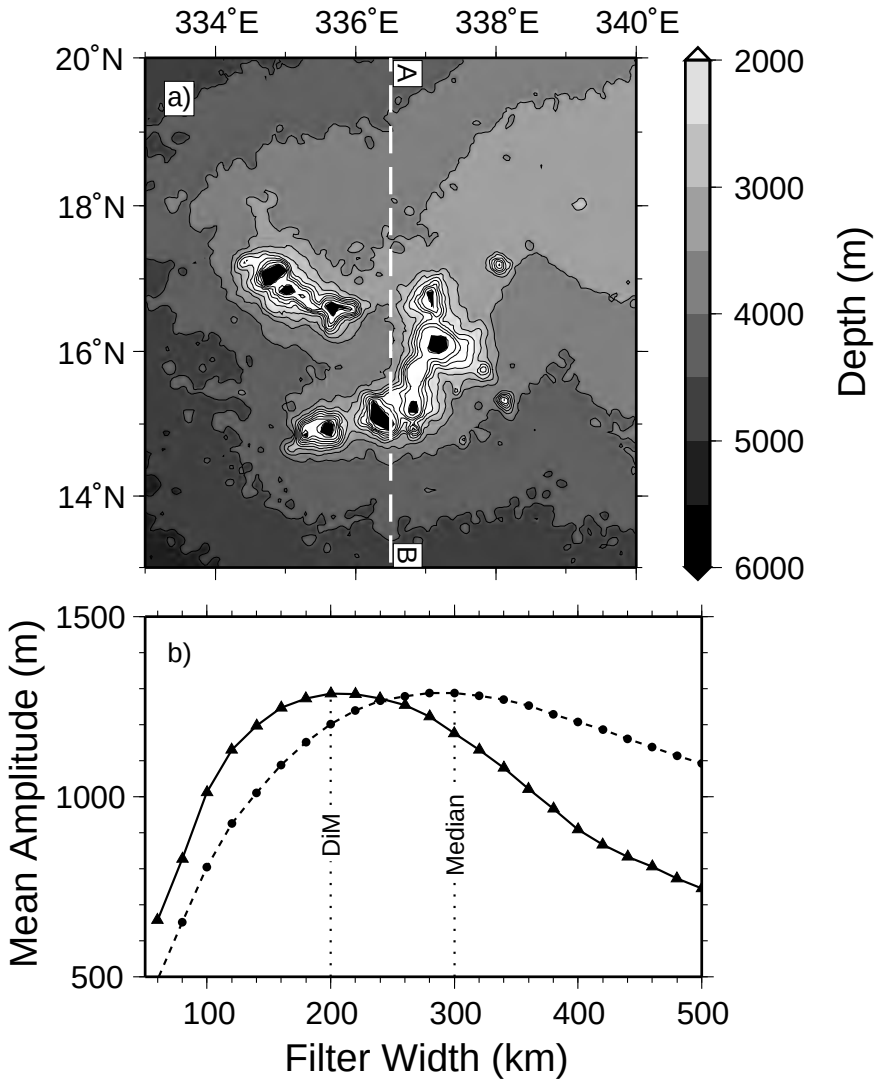

Figure 3.1: Bathymetry and the variation of mean amplitude ($\overline{d}$) estimated in the Cape Verde Islands region. a) Predicted bathymetry based on altimetry-drived gravity data [*Smith and Sandwell*, 1997]. The original and regional depths obtained by both the DiM and median filters are compared along profile AB (white dashed line) in Figure 3.2. The contour interval is 500 m. b) Variation of mean amplitudes calculated by the DiM (solid line with triangles) and median (dashed line with circles) filters. The volume and area of residual fields were evaluated in the domain defined by the $d(x, y) = 300$ m contour. Effective filter widths are 200 km and 300 km for the DiM and median filters, respectively.

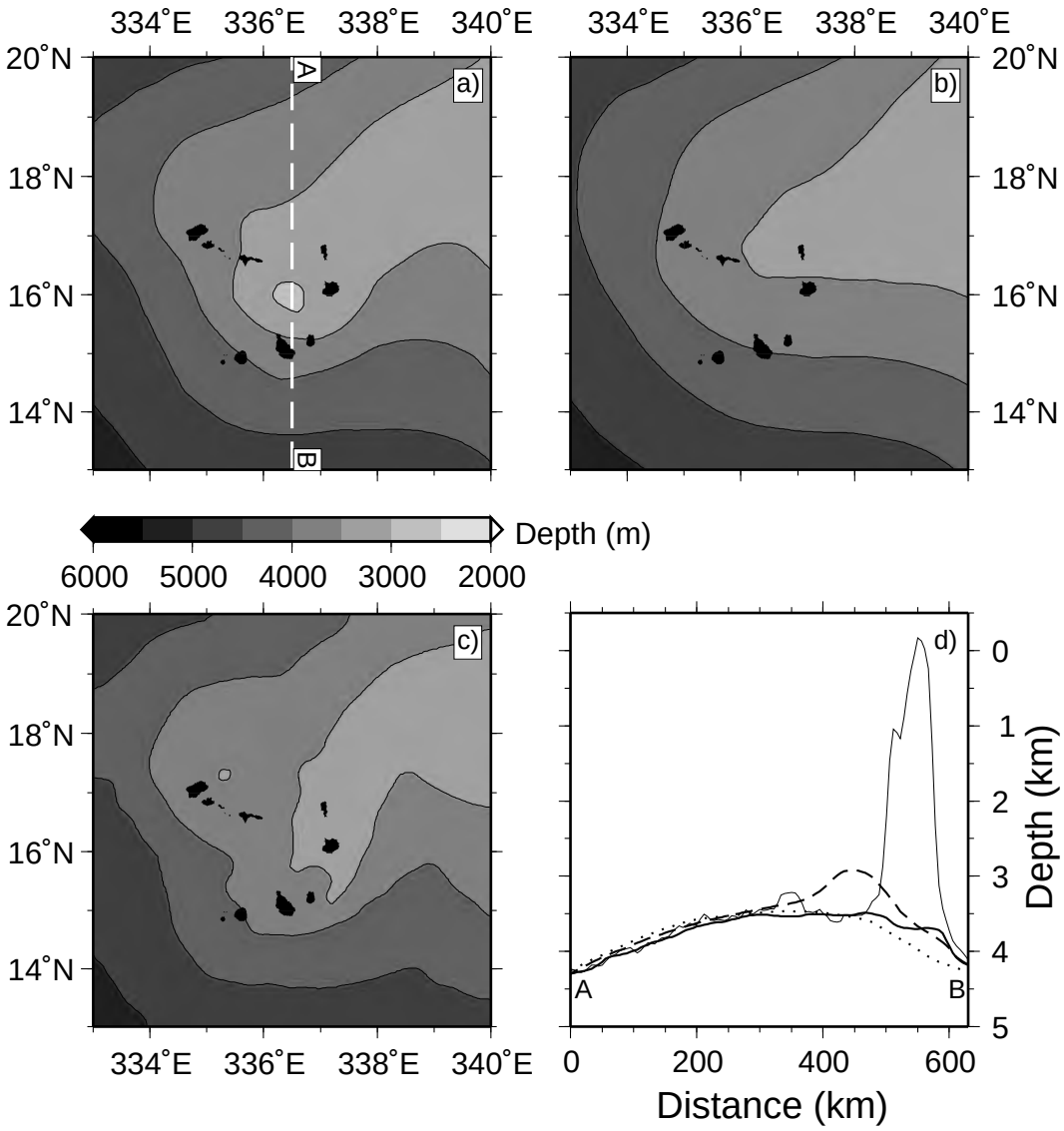

Figure 3.2: Estimated regional components in the Cape Verde Islands region. a) Regional component obtained by the spatial median filter with its effective filter width ($W = 300$ km). The white dashed line shows profile AB. b) Regional component obtained by the spatial median filter with the effective filter width ($W = 500$ km) from the study of *Ali et al.* [2003]. c) Regional component obtained by the DiM filter with its effective filter width ($W = 200$ km). Note that the DiM filtered data highlights many details of the swell apparent in the bathymetry (Figure 3.1a). d) Comparison of the original (thin solid line), median-filtered with $W = 300$ km (dashed line) and $W = 500$ km (dotted line), and DiM-filtered (thick solid line) bathymetric data along profile AB. The "pull-up" problem shows up very clearly in the dashed line and made *Ali et al.* [2003] use $W = 500$ km.

regional component with the original bathymetry. In this respect, the median filter with $W = 300$ km (Figure 3.2a) captured some details of the swell only in the northern area. The environment around the Islands (shaded black) is analogous to the case tested in Figure 2.2a because the Islands are on the southern part of the swell, sloping from its center to the south. Consequently, the errors (i.e., "pull-ups") in this regional component (dashed line in Figure 3.2d) resulted in an unacceptable separation [*Ali et al.*, 2003]. Note that the amplitude of the "pull-up" reached about 700 m, which clearly overestimates the amplitude of the swell. To reduce these errors, *Ali et al.* [2003] introduced a median filter with $W = 500$ km and produced a regional component as shown in Figure 3.2b. Although this compromise filter width reduced the errors (dotted line in Figure 3.2d), the overall regional component is biased because a major portion of the data input to the median filter does not reflect the actual trend beneath the features (Figure 3.2b). However, the DiM filter with $W = 200$ km returned many details of the swell (Figure 3.2c), compatible with its shape in the original bathymetry. The DiM filter successfully recovered the shape of the swell beneath the Islands (e.g., thick solid line in Figure 3.2d) using shorter filter width.

In the study by *Ali et al.* [2003], the residual component based on their estimated regional component (Figure 3.2b) was used to define the surface loads; these place limits on the magnitude of flexural deformation around the Cape Verde Islands. Because the regional component estimated by the conventional median filter (using $W = 500$ km) in this study is compatible with that used by *Ali et al.* [2003] to isolate the Cape Verde Islands, I can approximate the differences between the surface loads derived from their filtering and those from the DiM filtering (Table 3.1). As shown in Figure 3.2d, the estimated regional component of *Ali et al.* [2003] from the median filter (dotted line) are slightly deeper than expected, leading to overestimation of the total volume (by about 12%) for the surface loads with respect to that from the DiM filter. As *Ali et al.* [2003] used a constant density for the loads (i.e., 2700

kg/m^3), this difference would have propagated into the estimation of elastic thickness. However, the trade-offs with other model parameters (e.g., Young's modulus) in the flexural modeling process have not been investigated yet, but could lessen the effect of the overestimated mass. Furthermore, the basal areas of the surface loads were also overestimated (by about 28%). Although the wavelength of flexural deformation is mainly determined by the density of the material filling in the flexural moat, the overestimated area may still affect the flexural wavelength. The Cape Verde swell was approximated by the estimated regional components (Figure 3.2b and c). If one is interested in estimating the volcanic volume associated with the swell using the median-based regional component, the result will be underestimated by about 20%.

Table 3.1: Comparison of regional-residual separation obtained by the DiM and conventional median filters in the Cape Verde Islands region. To avoid the noise floor (i.e., the rough fabric of the seafloor), the volume and area of each estimated residual component (i.e., seamounts) were evaluated for the domain inside the 300 m contour. Swell amplitude is the difference between minimum and maximum depth in each regional field.

Filter	Volume (km^3)	Area(km^2)	Swell amplitude (m)
Median [*Ali et al.*, 2003]	10×10^4	9.5×10^4	1905
DiM	8.8×10^4	6.8×10^4	2408

As expected, the results of the DiM filters for the Cape Verde Islands region shows many similarities with those for the synthetic data sets in Figures 2.2 and 2.4. In these examples, the length scales of short-length-scale and background features did not overlap significantly. Furthermore, the Cape Verde Islands region is relatively small and clearly exhibits short-length-scale features (i.e., the Islands) on top of a long-length-scale background (i.e., the swell). Next, I apply the DiM filtering procedure with the MAD estimation outlined in the previous chapter to a more complex area: the seafloor around the Easter-Salas y Gomez Seamount Chain (Figure 3.3).

The test area mainly consists of voluminous seamounts (the Easter-Salas y Gomez Seamount Chain), an elongated volcanic ridge (the Nazca Ridge), a dislocated plate

exhibiting abrupt changes in age and water depth (the Nazca Fracture Zone), and both gentle (thermal subsidence of the lithosphere) and steep (the Peru-Chile Trench) slopes (Figure 3.3). In particular, the analysis of the Nazca plate is complicated by the superposition of at least two different types of slopes associated with the Peru and Chile Basins and the Nazca Ridge. Consequently, describing the distribution of depths around isolated bathymetric highs is key to a satisfactory separation for the Easter-Salas y Gomez Seamount Chain (ESC) region.

To apply the residual component directly to a planned flexure study, the shipboard multibeam bathymetric data available for the study area, including the swath data collected during Leg 6 of the 2001 Drift Expedition [*Naar et al.*, 2002] and SO146-GEOPECO [*Hampel et al.*, 2004], were compiled with a grid spacing of 30 arc seconds. As shown in the inset of Figure 3.3, the multibeam coverage is focused on the western [e.g., *Hey et al.*, 1995] and eastern [e.g., *Hampel et al.*, 2004] borders of the plate. The main trend of the ESC was defined by the predicted global bathymetry from the satellite altimetry data [*Smith and Sandwell*, 1997], which filled in areas outside the shipboard coverage. For the same reasons as above, this data domain was also extended by 5° in all directions using the predicted depths [*Smith and Sandwell*, 1997]. Because the smallest details in the 30 arc second data set, mainly contributions from the shipboard data, are not associated with the regional component, the DiM filtering operated on the bathymetric data resampled at a grid spacing of 5 arc minute (5 nautical mile) using bicubic interpolation [*Wessel and Smith*, 1995]. All data points on land were ignored by flagging them to have no data after the analysis.

The mean amplitude technique was first employed to determine effective filter widths (Figure 3.4). However, the mean amplitude did not approach a unique maximum for either the DiM or the conventional median filters. This result reaffirms my conclusion that this measure depends strongly on the bathymetry in question (e.g., Figure 2.5). In the case of the ESC region, the main reasons may be the complexity of

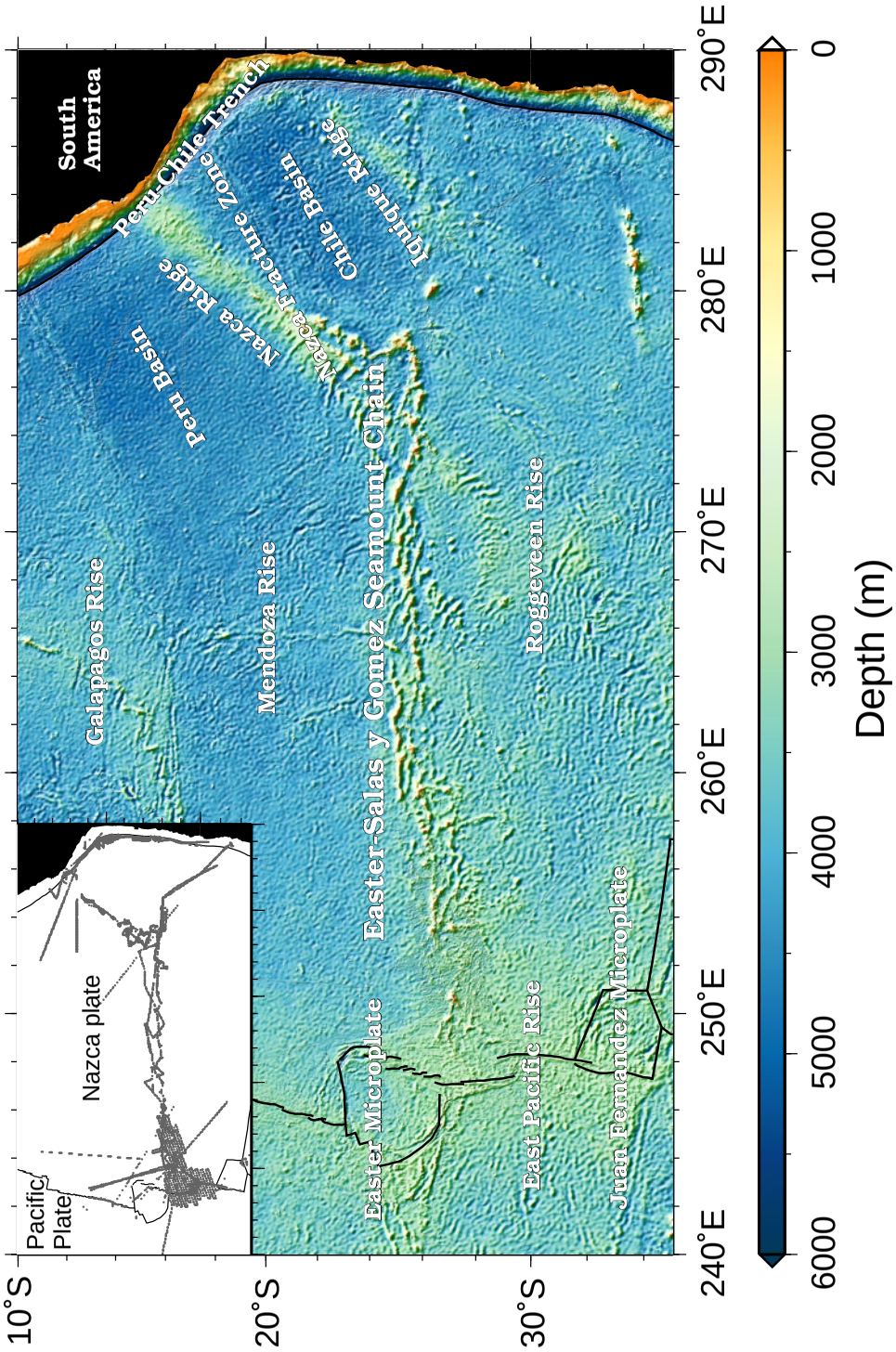

Figure 3.3: Bathymetric map and tectonic features of the Nazca plate. The areas shaded gray in the inset represent the coverage of the multibeam bathymetric data compiled in this study. Areas outside the coverage are filled with the predicted global bathymetry [*Smith and Sandwell*, 1997].

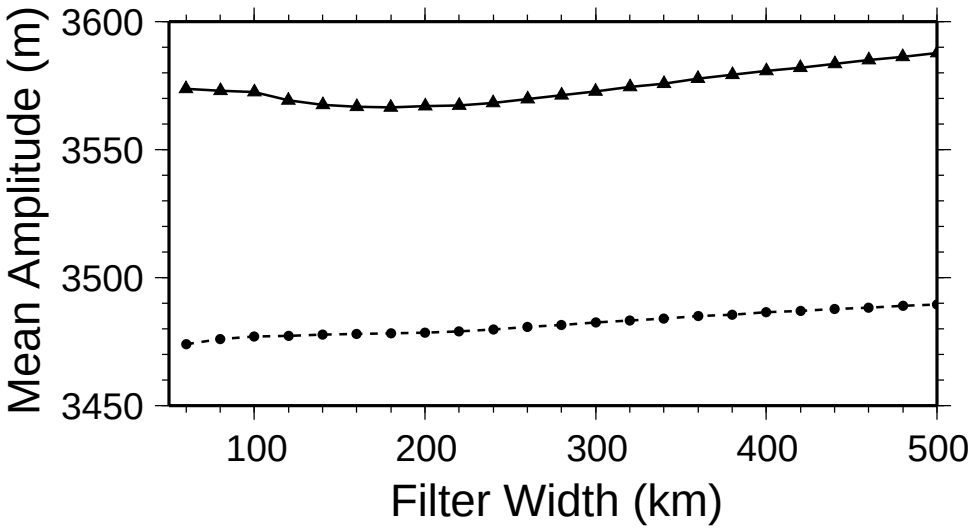

Figure 3.4: Variation of mean amplitude ($\overline{d}$) estimated in the Easter-Salas y Gomez Seamount Chain region. The mean amplitudes were calculated by the DiM (solid line with triangles) and median (dashed line with circles) filters. The volume and area of estimated residual components were evaluated in the domain defined by the $d(x, y) = 300$ m contour. Notice that there is no unique maximum in the mean amplitude.

the Nazca plate bathymetry and the relatively large filtering domain. Furthermore, it seems that the ridges and basins contribute to the growth in volume and area of the estimated residual components, respectively, and hence the ratio continues to increase monotonically as the filter width is increased. Based on the qualitative rule in (2.1) [*Wessel*, 1998], therefore, the largest seamount in the ESC area (with $D = 100$ km) was used instead to decide a range of effective filter widths, i.e., $W = 150 \pm 25$ km. To allow enough variation of estimated regional components, the uncertainty was determined empirically. Then, following the procedures outlined in the previous chapter, a regional component, $\tilde{f}(x, y)$, and MAD values, $\tilde{\sigma}(x, y)$, were estimated with W_i (in km), which is given by

$$W_i = \{125,\ 130,\ \cdots,\ 150,\ \cdots,\ 170,\ 175\}.$$

For all DiM-filtered data, the smoothing process using the spatial median filter with $W = 50$ km was applied before finding the median trend, $\tilde{f}(x, y)$.

In Figure 3.5a, the background features of the ESC area are emphasized by contouring depths below 3000 m. With the same shading scale and contour limits, the regional component, $\tilde{f}(x, y)$, in Figure 3.5b obtained by the DiM filtering scheme also traces many details of those features, including the East Pacific Rise, the Mendoza, Galápagos, and Roggeveen Rises, the Peru and Chile Basins, the Nazca and Iquique Ridges, and the Peru-Chile Trench (Figure 3.3). The uncertainties of the separation at each data point of the ESC region are shown by the distribution of MAD values (Figure 3.6). Overall, MAD values are less than 600 m. The scattered closed contours seem to be correlated with rough bathymetric fabric. Along the four profiles shown (solid lines), the filtered results for each effective filter width are compared, allowing inspection of areas of high MAD values. For profile 1, two seamounts were formed in close proximity to each other. As the sum of their individual length scales did not fall

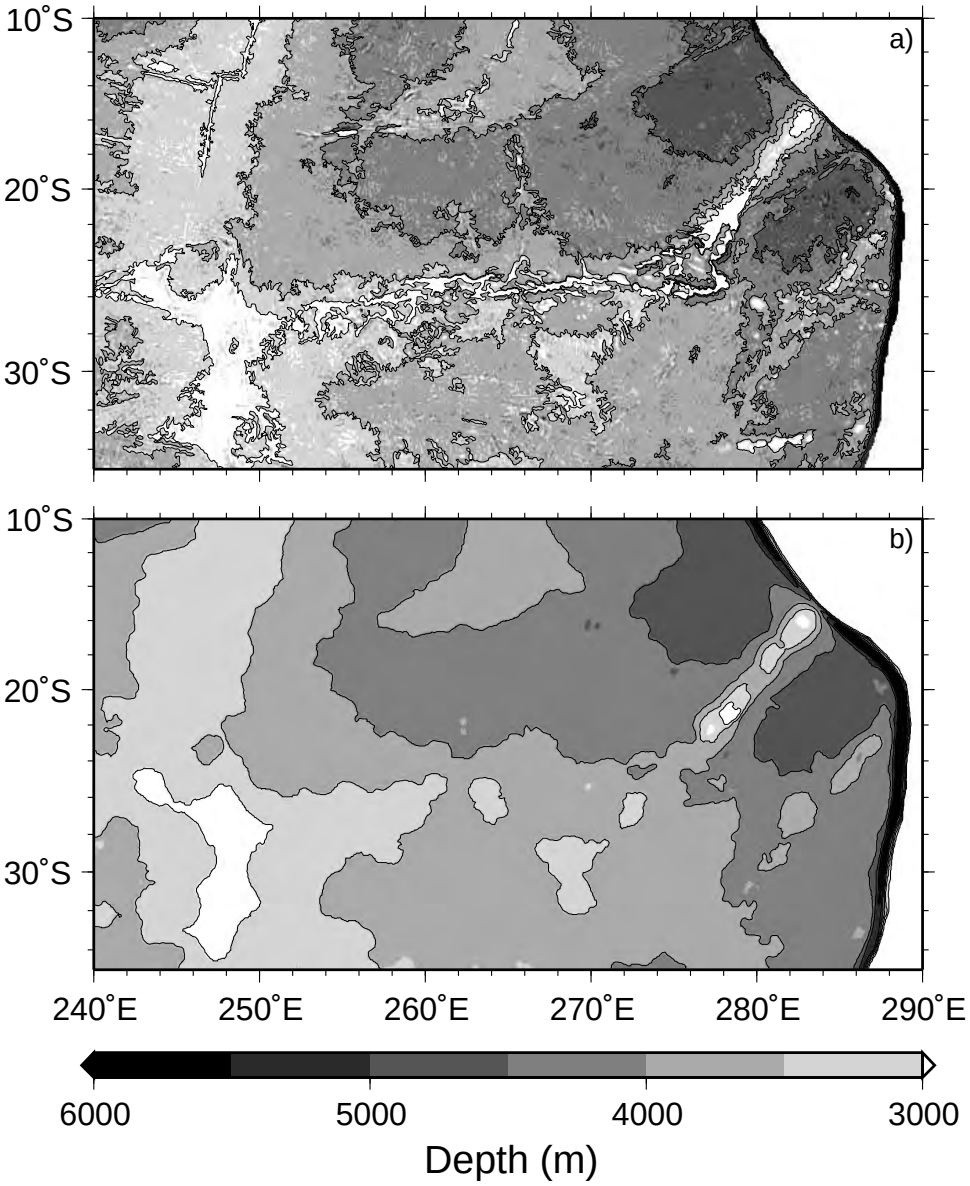

Figure 3.5: Bathymetry and estimated regional component of the Nazca plate. a) Bathymetric map of the Nazca plate in a gray scale. Depths between 8000 m and 3000 m are shown in order to highlight the background features. b) Regional component obtained by the DiM filtering of the data displayed in a). The contours at 500 m intervals in the estimated regional component depict most of the background features apparent in the upper panel.

into the range of effective filter widths, the DiM filters were not able to trace their bases. As predicted above, profiles 2 and 3 clearly exhibit the "pull-down" patterns along the axes of the Nazca and Iquique Ridges, respectively, as the filter widths were spanned. It is interesting that the Iquique Ridge shows up so clearly in the MAD image, whereas it was not particularly prominent in the original bathymetry (Figure 3.3). However, owing to its narrow width, the DiM filters were not able to follow the slopes of the Iquique Ridge as well as they did for the Nazca Ridge (profile 2), resulting in a wider regional component than the original data (profile 3). Profile 4 is evidence that DiM filters are able to follow steep slopes in real bathymetric data (e.g., the Peru-Chile Trench). The depth changes of the uplifted seafloor along the Peru-Chile Trench are too short in length-scale to be filtered out by the DiM filters, within the range of filter widths.

Obviously, DiM filters are not dynamic enough to fit every length scale within a complex filtering domain, as illustrated by the above examples. A researcher must therefore make a trade-off in the choice of filter width if a domain contains several different and overlapping length scales. In this study, the filter widths were limited to prevent the DiM filter from removing the Nazca Ridge. However, one may circumvent this problem by filtering small areas of interest separately. For example, studies to understand the thermomechanical properties of oceanic lithosphere could break the study region into small areas for modeling [e.g., *Kruse et al.*, 1997]. Thus, the separation can be made more robust in those boxes by minimizing such compromises on effective filter widths.

A residual component of the Nazca plate was obtained by subtracting the estimated regional component (with 30 arc second grid spacing) from the bathymetric data (Figure 3.7). Notice that regions surrounding the Easter-Salas y Gomez Seamount Chain exhibit variations between -500 m and 500 m, corresponding to the rough bathymetric fabric of the Nazca plate. Thus, volcanic loads can be regarded as being positive

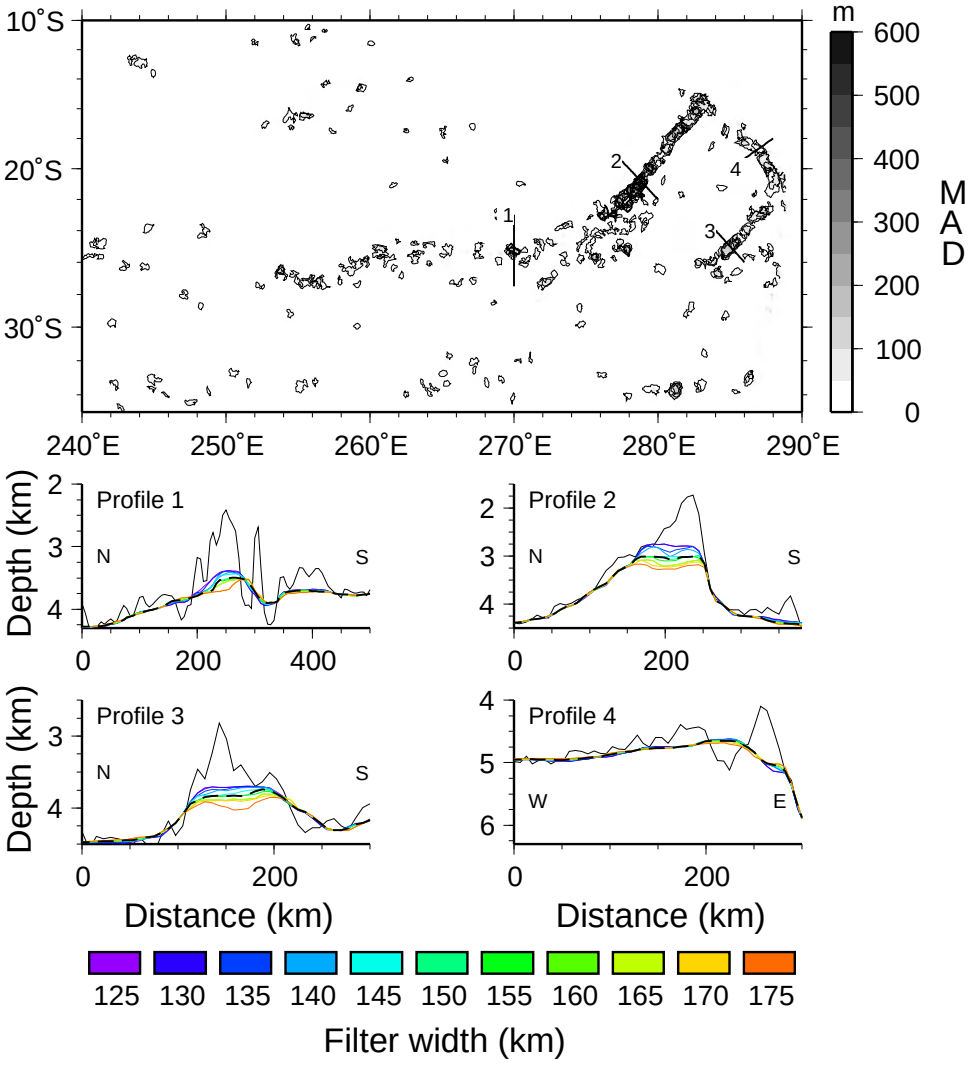

Figure 3.6: Uncertainties of the separation obtained by the DiM filters. The map shows the distribution of MAD (median absolute deviation) values as the robust estimate of variation in the regional component. The variation of the DiM filtering output for different filter widths (color bar at the bottom) is compared for four selected profiles. Profile 1: Two closely located seamounts form a longer-length-scale feature that the DiM filters do not completely remove with the given filter range. Profile 2: As shown in Figure 2.5, pull-downs are found along the Nazca ridge. Profile 3: The pull-downs along the Iquique ridge make it more noticeable in the map of MAD than in the bathymetric map. Profile 4: The DiM filters are able to follow the steep slope of the Peru-Chile trench. The rifted areas caused by the rigidity of the plate are large enough to be separated.

departures from a flat surface which then serves as the standard reference level for flexure modeling. One should consult the MAD values before using the information from the estimated residual component because of possible underestimation (e.g., profile 1 in Figure 3.6). For instance, some negative residual amplitudes (about −6000 m) near the Easter Microplate are a result of the deformation of rotating seafloor, such as Pito Deep [*Hey et al.*, 2002], and are unrelated to flexural loading.

The Easter-Salas y Gomez Seamount Chain (ESC) is a prominent bathymetric feature on the Nazca plate. Although its origin is still not fully understood, the hot spot model has been accepted as an explanation for the surface volcanism [e.g., *O'Connor et al.*, 1995; *Kruse et al.*, 1997]. To test various models for the formation of the ESC region, *Kruse et al.* [1997] used the flexure model to estimate elastic thicknesses along the chain. An estimate of elastic thickness indicates the strength of the lithosphere at the time the seamounts formed and hence the thermal structure or the age of the lithosphere at that time [*Wessel*, 1992; *Kruse et al.*, 1997; *McNutt et al.*, 1997]. As mentioned above, flexural deformation is a lithospheric response to a surface load (e.g., seamounts), which must be defined first [e.g., *Ali et al.*, 2003]. However, *Kruse et al.* [1997] estimated the load by including all materials above a chosen depth contour (i.e., 3000 m). Among the several subregions they studied, I consider boxes 1 and 2 (Figure 3.7) to compare the differences in estimation of the surface loads (Table 3.2). In box 1 (centered at the Easter Island) the total volume and area of my residual features are significantly smaller (by about 40%) than that used by *Kruse et al.* [1997]. However, the differences for box 2 (i.e., Salas y Gomez Island) are relatively small. Based on the estimated components of these boxes, it seems that the background trend of box 1 exhibits a relatively steep slope, whereas that of box 2 is nearly flat. Thus, for box 2 the constant depth contour applied by *Kruse et al.* [1997] is able to separate seamounts compatiable with DiM filtering, but not for box 1. For these areas, it is unclear if the flexure modeling using my residual

component will result in estimates incompatible with the previous work. Moreover, using a unform density for the surface load tends to affect estimates of flexural model parameters [*Minshull and Charvis*, 2001]. A careful examination is necessary in order to investigate possible biases most likely associated with uncertainties of surface loads (i.e., the residual components).

Table 3.2: Comparison of the surface loads from regional-residual separation using the DiM filtering technique and a 3000 m depth contour in the Easter-Salas y Gomez Islands region. To avoid the noise floor, the volume and area of the estimated residual component (Figure 3.7) were evaluated for the domain inside the 300 m contour. Following *Kruse et al.* [1997], bathymetric features (Figure 3.3) above the 3000 m depth contour were included to estimate the volume and area.

	Box 1	Box 2
Kruse et al. [1997]		
Volume (km^3)	6.6×10^3	8.0×10^3
Area(km^2)	1.1×10^4	1.2×10^4
DiM filter		
Volume (km^3)	4.6×10^3	7.3×10^3
Area(km^2)	0.7×10^4	1.2×10^4

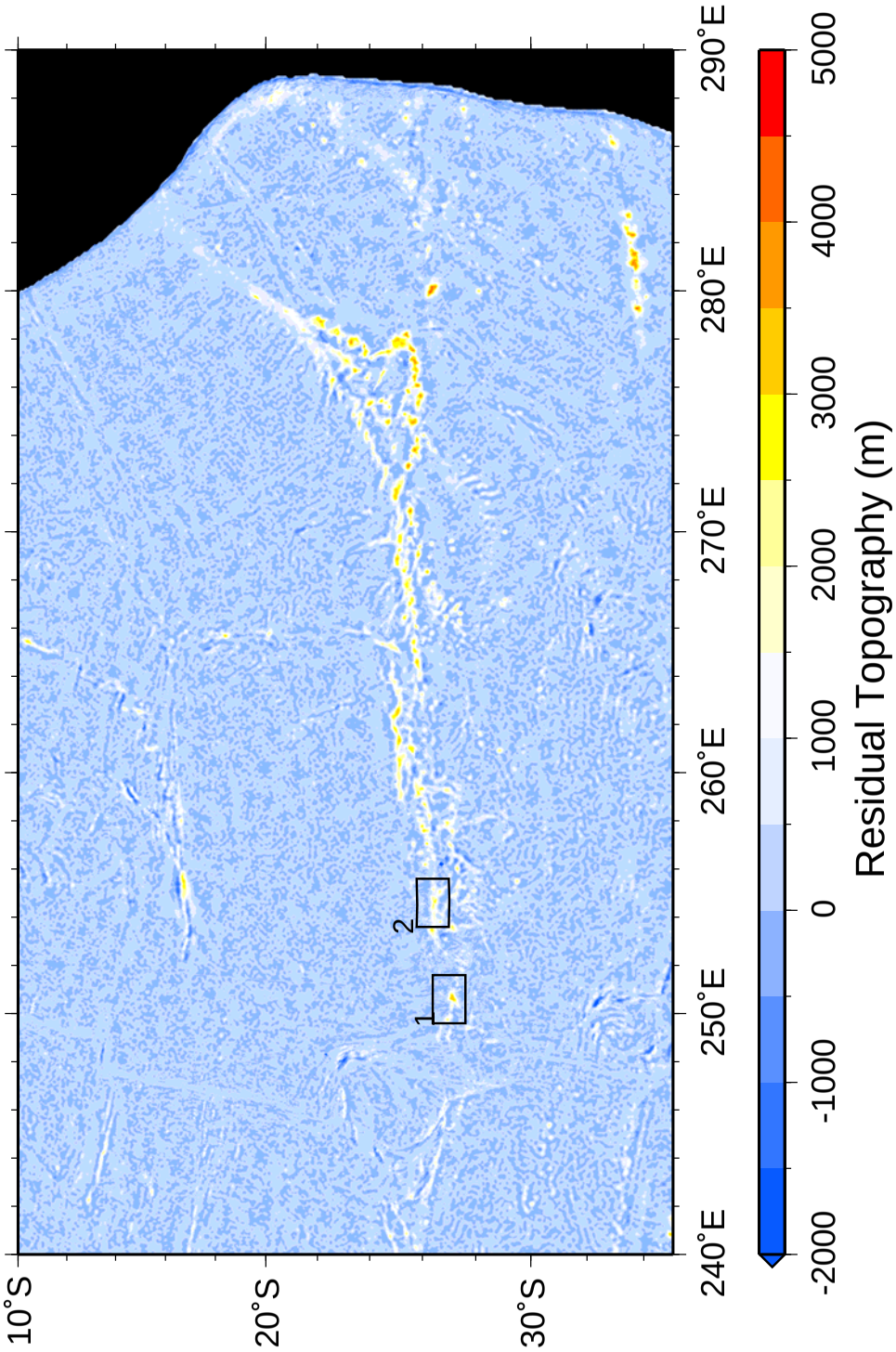

Figure 3.7: Estimated residual topography of the Nazca plate. The seamounts are separated from the other bathymetric features of the Nazca plate, so the surrounding depths range mostly between −500 m and 500 m. Boxes 1 and 2 are the same as the areas where *Kruse et al.* [1997] estimated elastic thicknesses. Land is shaded black.

Chapter 4

Discussion

The DiM filters preserve the basic characteristics of spatial median filters, such as the insensitivity to outliers (i.e., robustness), and overcome the shortcoming of conventional median filters to produce biased filtered data if the data contain a sloping background. The modification using bow-tie sectors was made in order to reduce the effects of the sloping regional component on determining median values. An alternative to sectoring may be to remove the sloping component first, before median filtering the data. However, bathymetry exhibits various slopes caused by different geologic phenomena. Although the area of interest has only small-length-scale features (e.g., seamounts), the background seafloor would represent the typical depth variation resulting from thermal subsidence of the lithosphere. In such situations, the GDH1 thermal subsidence model [*Stein and Stein*, 1992] can be used to remove some of the background features. Experiments with the GDH1 model on the real bathymetric data, however, led to unacceptable separation results. Furthermore, the model itself is sensitive to the separation of "normal" seafloor from anomalous bathymetric features, including oceanic plateaus, swells, and seamounts [*Stein and Stein*, 1992; *Hillier and Watts*, 2005]. For this reason, the DiM filtering technique seems to be an effective and efficient way to allow median filters to estimate an unbiased regional component. To remedy the problem of using median filters on data with a sloping background, I have focused on 3-D spatial filters, because regional-residual separation in a 2-D data set will be biased because of limited information about the third dimension. However, the bow-tie sectors of the DiM filter become identical to normal median filters for 2-D profile data (e.g., Figure 2.2a). For such cases, removing the best-fitting plane from the data using least-squares fit may be the best

solution [*Wessel*, 1998].

The MAD analysis used in the regional-residual separation was developed in order to estimate uncertainties in DiM filtered data. No computational method can completely separate two components from observed data, unless the exact shape of one of the components is known or they are completely without overlap in either the spatial or wavenumber domains. In other words, one cannot argue that the computed result is the "true" residual component. However, the variations of separated components resulting from different filter widths can be observed in the spatial domain. In this respect, the MAD values approximate errors associated with estimating a regional component, which propagate into a residual component through (2.7). The arithmetic mean easily can be biased by outliers; hence, so can the standard deviation. The MAD, thus, is a robust estimator that is well suited to represent the fluctuations in filtered data.

A robust alternative to both the DiM and median filtering for regional-residual separation is mode filtering. The mode filter searches for the value that occurs with the greatest frequency in the data within the filter window. For this reason, the mode filter can outperform the median filter when the data are strongly affected by outliers in the data [*Smith*, 1990; *Levitt and Sandwell*, 1996; *Sichoix and Bonneville*, 1996; *McNutt et al.*, 1996]. However, I found from considerable testing with the mode filter on real geophysical data that the mode filter is more unstable than the median filter [e.g., *Wessel*, 1998]. Based on simple inspection of the data distribution, the data inside a filter window can have several distinct modes. In particular, mode-filtered data represent stair-like regional trends causing systemic biases when using such trends to define the bases of seamounts. I also attempted to combine mode filters with bow-tie sectors as the mode filter also tends to be affected by a sloping background [*Wessel*, 1998]. However, the data inside each bow-tie sector also may have several modes. It is not obvious that the mode filter has any specific and

unique properties associated with short-length-scale features, whereas the median filter does, as shown in (2.1). This unpredictable pattern of the mode filter hampers the application of the bow-tie sectoring scheme as the way to select a representative mode value from numerous modes cannot be established clearly. A careful analysis of mode filters is needed to address this predicament. Thus, for the time being, I prefer the median-based filter over the mode filter.

The estimated regional and residual components of the bathymetry can be used to investigate various geologic phenomena. For example, the estimated regional component provides the details of the shape and size of swells (e.g., Figure 3.2) and hence allows researchers to estimate the mass anomaly associated with a swell, which is proportional to its width and mean amplitude [e.g., *Vidal and Bonneville*, 2004; *Adam et al.*, 2005]. Furthermore, characterization of depth anomalies (i.e., swells) is directly applicable to studying the relationship between the seafloor depth and age; understanding this relationship requires the depths associated with the thermal subsidence of a plate [e.g., *Parsons and Sclater*, 1977; *Stein and Stein*, 1992; *Hillier and Watts*, 2005]. In studies of the flexural deformation of oceanic lithosphere caused by volcanic loads (e.g., seamounts), however, the estimated residual component is a measure of surface loads (e.g., Figure 3.7). Although seamounts are generally emplaced on sloping backgrounds (e.g, from thermal subsidence of the lithosphere), most flexural studies estimate the amount of the surface load by simply including the material above a chosen constant level (i.e., mean depth around the feature) [e.g., *Watts and ten Brink*, 1989; *Kruse et al.*, 1997]. In particular, flexural studies often yield incorrect results when the surface loads are placed on top of a swell because parts of the swell are incorrectly taken into account in the volume computation [e.g., *Watts and ten Brink*, 1989; *Wessel*, 1993]. All previous studies concerned with the above topics have assumed no error in defining regional or residual components and hence no errors were propagated to errors in the final estimation of model parameters (e.g., elastic

parameters and buoyancy flux). For example, the flexure model predicts the deflection of an oceanic plate for a given surface load, and these deflections depend strongly on the thickness of the plate. To place limits on the flexural model parameters, the model computes free-air gravity anomalies resulting from both the surface load and the deformed crust, and compares them with observed data. In this process, uncertainties in the shape of the surface load (i.e., the estimated residual component) are usually not considered, although its shape defines the total mass of the load deflecting the plate and produces gravity anomalies from both the surface and subsurface (i.e., flexed crust) boundaries. Further experimentation with uncertainties obtained by the MAD analysis would allow for better representation of geophysical models associated with bathymetric features.

Numerous approaches can be made to isolate features of interest (e.g., swells or seamounts) from bathymetric data [e.g., *Yuen et al.*, 2002; *Hillier and Watts*, 2004; *Adam et al.*, 2005]. However, the separation procedures including several subjective criteria make it difficult to produce a unique separation result. This limitation also prevents researchers from determining how errors in the input data propagate into estimates of key model parameters. Because DiM filtering applies median filters to each sector, one benefit of the DiM filtering method is that the separation results are reproducible. It means that one can replicate either suitable or unsuitable results obtained by the DiM filters. These variations are quantified by the MAD values. Thus, the DiM filtering and associated MAD analysis may enable us to reduce the ambiguity of determining suitable input data (i.e., regional or residual components), characterize their uncertainties, and better quantify estimates of geophysical model parameters.

Chapter 5

Conclusions

From this study, I draw the following conclusions.

1. The directional median (DiM) filter is established as an alternative to conventional spatial median filters which are often unable to remove short-length-scale features (e.g., seamounts) superimposed on sloping backgrounds (e.g., swells). By dividing the filter circle into the eight bow-tie sectors, the DiM filter is able to return median values unaffected by the slope, hence overcoming this limitation.

2. Uncertainties of regional-residual separation are quantified by the median absolute deviation (MAD) analysis to examine whether the DiM filters produce similar regional trends within an appropriate range of effective filter widths. Based on the distribution of MAD values, one can pinpoint the causes of large MAD values and reduce them by comparing them with the original bathymetric data.

3. The DiM filtering scheme resulted in successful separations of bathymetric data in the vicinity of the Easter-Salas y Gomez Seamount Chain and Cape Verde Islands. These results confirm that the DiM filtering scheme is an efficient and effective tool for regional-residual separation.

Bibliography

Adam, C., V. Vidal, and A. Bonneville (2005), MiFil: A method to characterize seafloor swells with application to the south central Pacific, *Geochem. Geophys. Geosyst.*, *6*, Q01003, doi:10.1029/2004GC000814.

Ali, M. Y., A. B. Watts, and I. Hill (2003), A seismic reflection profile study of lithospheric flexure in the vicinity of the Cape Verde Islands, *J. Geophys. Res.*, *108*(B5), 2239, doi:10.1029/2002JB002155.

Crough, S. T. (1983), Hotspot swells, *Ann. Rev. Earth Planet. Sci*, *11*, 165–193.

Davis, J. C. (1986), *Statistics and Data Analysis in Geology*, 2 ed., John Wiley, New York.

Hampel, A., N. Kukowski, J. Bialas, C. Huebscher, and R. Heinbockel (2004), Ridge subduction at an erosive margin: The collision zone of the Nazca Ridge in southern Peru, *J. Geophys. Res.*, *109*, B02101, doi:10.1029/2003JB002593.

Hey, R. N., P. D. Johnson, F. Martínez, J. Korenaga, M. L. Somers, Q. J. Huggett, T. P. LeBas, R. I. Rusby, and D. F. Naar (1995), Plate boundary reorganization at a large-offset, rapidly propagating rift, *Nature*, *378*, 167–170.

Hey, R. N., F. Martínez, S. Diniega, D. F. Naar, J. Francheteau, and the Pito93 Scientific Team (2002), Preliminary attempt to characterize the rotation of seafloor in the Pito Deep area of the Easter Microplate using a submersible magnetometer, *Marine Geophys. Res.*, *23*, 1–12.

Hillier, J. K., and A. B. Watts (2004), "Plate-like" subsidence of the East Pacific Rise - South Pacific superswell system, *J. Geophys. Res.*, *109*, B10102, doi: 10.1029/2004JB003041.

Hillier, J. K., and A. B. Watts (2005), Relationship between depth and age in the North Pacific Ocean, *J. Geophys. Res.*, *110*, B02405, doi:10.1029/2004JB003406.

Kruse, S. E., Z. J. Liu, D. F. Naar, and R. A. Duncan (1997), Effective elastic thickness of the lithosphere along the Easter Seamount Chain, *J. Geophys. Res.*, *102*(B12), 27,305–27,317.

Lambeck, K. (1981), Lithospheric response to volcanic loading in the southern Cook Islands, *Earth Planet. Sci. Lett.*, *55*, 482–496.

Lambeck, K., and S. M. Nakiboglu (1980), Seamount loading and stress in the ocean lithosphere, *J. Geophys. Res.*, *85*(B11), 6403–6418.

Levitt, D. A., and D. T. Sandwell (1996), Modal depth anomalies from multibeam bathymetry: Is there a south Pacific superswell?, *Earth. Planet. Sci. Lett.*, *139*(1/2), 1–16.

McNutt, M., L. Sichoix, and A. Bonneville (1996), Modal depths from shipboard bathymetry: There is a south Pacific superswell, *Geophys. Res. Lett.*, *23*(23), 3397–3400.

McNutt, M. K. (1998), Superswells, *Rev. Geophys.*, *36*(2), 211–244.

McNutt, M. K., and H. W. Menard (1978), Lithospheric flexure and uplifted atolls, *J. Geophys. Res.*, *83*(B3), 1206–1212.

McNutt, M. K., D. W. Caress, J. Reynolds, K. A. Jordahl, and R. A. Duncan (1997), Failure of plume theory to explain midplate volcanism in the southern Austral islands, *Nature*, *389*(6650), 479–482.

Minshull, T. A., and P. Charvis (2001), Ocean island densities and models of lithospheric flexure, *Geophys. J. Int.*, *145*, 731–739.

Müller, R. D., W. R. Roest, J.-Y. Royer, L. M. Gahagan, and J. G. Sclater (1997), Digital isochrons of the world's ocean floor, *J. Geophys. Res.*, *102*(B2), 3211–3214.

Naar, D. F., K. T. Johnson, P. Wessel, and D. Pyle (2002), Preliminary Multibeam Mapping and Dredging Results Along the Nazca Ridge and Easter/Salas y Gomez Chain, *Eos Trans. AGU*, *Ocean Sci. Meet. Suppl.*(Abstract OS32O-11).

Nettleton, L. L. (1976), *Gravity and magnetics in oil prospecting*, McGraw-Hill, New York.

O'Connor, J. M., P. Stoffers, and M. O. McWilliams (1995), Time-space mapping of Easter chain volcanism, *Earth Planet. Sci. Lett.*, *136*, 197–212.

Parsons, B., and J. G. Sclater (1977), An analysis of the variation of ocean floor bathymetry and heat flow with age, *J. Geophys. Res.*, *82*, 803–827.

Rousseeuw, P. J., and A. M. Leroy (1987), *Robust regression and outlier detection*, John Wiley and Sons, New York.

Sichoix, L., and A. Bonneville (1996), Prediction of bathymetry in french polynesia constrained by shipboard data, *Geophys. Res. Lett.*, *23*(18), 2469–2472.

Smith, W. H. F. (1990), Marine geophysical studies of seamounts in the Pacific Ocean basin, Ph. D., Columbia Univ.

Smith, W. H. F., and D. T. Sandwell (1997), Global sea floor topography from satellite altimetry and ship depth soundings, *Science*, *277*(5334), 1956–1962.

Starck, J.-L., A. Bijaoui, I. Valtchanov, and F. Murtagh (2000), A combined approach for object detection and deconvolution, *Astron. Astrophys. Suppl. Ser.*, *147*, 139–149.

Stein, C. A., and S. Stein (1992), A model for the global variation in oceanic depth and heat flow with lithospheric age, *Nature*, *359*(6391), 123–129.

Telford, W. M., L. P. Geldart, R. E. Sheriff, and D. A. Keys (1986), *Applied Geophysics*, Cambridge Univ. Press, London.

Van Ark, E., and J. Lin (2004), Time variation in igneous volume flux of the Hawaii-Emperor hot spot seamount chain, *J. Geophys. Res.*, *109*, B11401, doi: 10.1029/2003JB002949.

Vidal, V., and A. Bonneville (2004), Variations of the Hawaiian hot spot activity revealed by variations in the magma production rate, *J. Geophys. Res.*, *109*, B03104, doi:10.1029/2003JB002559.

Watts, A. B., and U. S. ten Brink (1989), Crustal structure, flexure, and subsidence history of the Hawaiian islands, *J. Geophys. Res.*, *94*(B8), 10,473–10,500.

Wessel, P. (1992), Thermal stresses and the bimodal distribution of elastic thickness estimates of the oceanic lithosphere, *J. Geophys. Res.*, *97*(B10), 14,177–14,193.

Wessel, P. (1993), A reexamination of the flexural deformation beneath the Hawaiian Islands, *J. Geophys. Res.*, *98*(B7), 12,177–12,190.

Wessel, P. (1998), An empirical method for optimal robust regional-residual separation of geophysical data, *J. Math. Geol.*, *30*(4), 391–408.

Wessel, P., and W. H. F. Smith (1995), New version of the Generic Mapping Tools released, *Eos Trans. AGU*, *76*(33), 329.

White, R. S. (1993), Melt production rates in mantle plumes, *Philos. Trans. Phys. Sci. Eng.*, *342*, 137–153.

Yuen, D. A., A. P. Vincent, M. Kido, and L. Vecsey (2002), Geophysical applications of multidimensional filtering with wavelets, *Pure Appl. Geophys.*, *159*, 2285–2309.